Surface electronic structures of Ba overlayers on W(100), W(110), and W(111)

Z. A. Ibrahim* and M. J. G. Lee
Department of Physics, University of Toronto, 60 St. George Street, Toronto, Ontario, Canada M5S 1A7
(Received 5 February 2007; revised manuscript received 18 August 2007; published 22 October 2007)

The total energy distributions (TEDs) in field emission (FE) and photofield emission (PFE) and the work functions have been measured at room temperature for Ba adsorbed on W(100), W(110), and W(111) in the range of coverage from 0 to 1 ML (monolayer). We observe two initial state peaks and three final state peaks on W(100)/Ba, six initial state peaks and one final state peak on W(110)/Ba, and two initial state peaks and two final state peaks on W(111)/Ba. We extend the full-potential linear augmented plane wave method for the electronic structures of periodic lattices to calculate the emission current in FE and surface PFE at a metal-adsorbate-vacuum interface. Our calculations account for the energies of all of the initial state features observed experimentally in FE and surface PFE from clean W(100), in PFE and angle-resolved inverse photoemission spectroscopy from W(100)/Ba at 1 ML, and for all of the peaks observed in FE, surface PFE, and photoemission from W(110)/Ba at 0.6 ML and from W(111)/Ba at 1 ML. The dz^2-like surface states of the Swanson hump [L. W. Swanson and L. C. Crouser, Phys. Rev. Lett. **16**, 389 (1966)] of clean W(100) hybridize with *s*-like states of the $c(2\times2)$ overlayer and are shifted by −1.60 eV to yield a prominent peak in PFE. An isolated Ba $c(2\times2)$ layer is found to be weakly metallic; the metallicity is greatly enhanced when it is adsorbed on a W(100) substrate. The TEDs in PFE from the atomically less dense overlayer W(110)/Ba (2×2) are dominated by substrate-overlayer interactions, while those from the atomically denser overlayer W(111)/Ba (1×1) are dominated by interactions within the overlayer. Our results yield evidence that above 1/3 ML Ba coverage on W(111), which corresponds to a commensurate $(3^{1/2}\times3^{1/2})R30°$ overlayer, the interstitial sites fill in randomly to form a commensurate (1×1) overlayer at 1 ML coverage.

DOI: 10.1103/PhysRevB.76.155423 PACS number(s): 73.20.At, 73.20.−r, 79.70.+q

I. INTRODUCTION

Studies of the surface electronic structures of metal-adsorbate-vacuum interfaces are expected to reveal the types of bond formed, the role played in the bonding by surface states and surface resonances, and the charge shifts induced by the adsorbate overlayer. The electronic structures of metal-adsorbate-vacuum interfaces play an important role in such fields as epitaxy and heterogeneous catalysis, while electron emission from overlayers of alkaline-earth metals and their oxides is widely used for cathodes in discharge lamps and photoelectron emission devices because of its well-known effect in reducing the work function. The work function[1–6] and the diffusion[7–9] of Ba atoms adsorbed on tungsten have received a lot of attention, but relatively little work, either experimental or theoretical, has been published on electron emission at W-Ba-vacuum interfaces.

The first total energy distribution (TED) measurements in field emission (FE) from Ba atoms singly adsorbed on low-index surfaces of W were carried out by Plummer and Young.[10] Gadzuk[11] and Plummer and Young[10] argued that the interaction with the W substrate broadens the 6*s* valence states of atomic Ba and shifts them to lower energy, while the more localized 6*s*5*d* excited states are less affected. They attributed a peak observed in the TED in FE from Ba atoms singly adsorbed on W(110) at about −0.4 eV (energies are expressed relative to the Fermi level E_F) and on W(111) at about −0.7 eV to the broadened 6*s* Ba states, and they attributed two narrow peaks observed in the TED in FE from Ba atoms singly adsorbed on W(111) at −0.4 eV and −0.1 eV to the 6*s*5*d* states.

Radoń and Jaskólka[12] carried out photofield emission (PFE) measurements for W(100) at a Ba coverage much larger than that reported by Plummer and Young, but less than 1 ML (monolayer). Lamouri *et al.*[13] used angle-resolved inverse photoemission spectroscopy (ARIPS) to study the unoccupied states of W(100) with a 1 ML Ba overlayer.

TEDs from W(110) with Ba coverage in the range 0–0.6 ML have been measured in photoemission at normal emission by Pi *et al.*[14,15] using synchrotron radiation at 60 eV. The TEDs from clean W(110) show surface peaks at −1.41, −0.95, and −0.41 eV, as well as several bulk peaks at lower energies. Increasing the Ba coverage weakened these surface peaks and shifted them to lower energy, but no new peaks were observed.

Radoń and Jaskólka[12] have carried out PFE measurements for W(110) and W(111) at a Ba coverage of less than 1 ML. They observed two Ba-induced peaks just below E_F, at −0.07(2) and −0.28(4) eV.

Hemstreet and Chubb[16] carried out a full-potential linear augmented plane wave (FP-LAPW) calculation within the local density approximation for a five layer W(100) film with a Ba $c(2\times2)$ layer (corresponding to 1 ML coverage) on each side. The spin-orbit interaction was not included in their calculation. Lamouri *et al.*[13] carried out fully relativistic embedded-cluster calculations using muffin-tin potentials to calculate the electronic structure of a Ba $c(2\times2)$ overlayer deposited on two layers of W(100). To our knowledge, no other calculations for W with Ba overlayers have been reported in the literature.

In the present paper, we report room-temperature measurements of the TEDs of the emission currents in PFE from Ba overlayers on W(100) [denoted W(100)/Ba] in the range of coverage from 0 to 1 ML, on W(110) [denoted W(110)/Ba] in the range of coverage from 0 to 0.6 ML, and

on W(111) [denoted W(111)/Ba] in the range of coverage from 0 to 1 ML. In order to interpret the experimental data, we have carried out *ab initio* FP-LAPW calculations of the ***k***-resolved layer densities of states (K-LDOS), and of the TEDs of the emission current in FE and PFE from W(100), W(110), and W(111) with commensurate Ba overlayers. As our method of calculation involves the assumption of translational symmetry parallel to the surface, our W(100) calculations were carried out with a Ba $c(2\times2)$ overlayer [denoted W(100)/Ba $c(2\times2)$], which corresponds to 1 ML coverage. Low-energy electron diffraction (LEED) measurements[2,6] have shown that at 1 ML coverage, the Ba atoms on W(110) arrange in an incommensurate hexagonal close-packed structure with an atomic density of 6.2×10^{14} atoms cm^{-2}. Our W(110) calculations were carried out with a Ba (2×2) overlayer [denoted W(110)/Ba (2×2)], which corresponds to 0.6 ML coverage and is known to be the commensurate overlayer that is closest to 1 ML coverage.[2] Our W(111) calculations were carried out with a Ba (1×1) overlayer [denoted W(111)/Ba (1×1)], which corresponds to 1 ML coverage.

The following are, to our knowledge, all unique features of the present paper. We report the experimental observation of two initial state peaks F_1 and G_1, and two final state peaks J_1 and K_1 in FE and PFE from W(100)/Ba. In addition, we present the calculations of the emission current in FE and surface PFE from a metal-overlayer-vacuum interface. In contrast to previously reported calculations of the surface electronic structure of W(100)/Ba $c(2\times2)$, the transition from the surface to the bulk is represented more adequately by seven W layers as compared with three[16] or two[13] W layers. Our results account for the energies of all of the initial state features observed experimentally in FE, PFE, and ARIPS.[13] Dispersion curves in a representative direction for clean W(100), an isolated Ba $c(2\times2)$ layer, and W(100)/Ba $c(2\times2)$ are presented to show how the ***k***-resolved surface electronic structure is modified by the substrate-overlayer interaction. We find that the substrate-overlayer interaction greatly enhances the metallicity of a Ba overlayer on W(100) at monolayer coverage.

We also report experimental studies of the TEDs in FE and PFE from W(110)/Ba with coverage up to 0.6 ML and from W(111)/Ba with coverage up to 1 ML. Two final state peaks L_2 and M_2 are observed on W(110)/Ba, as well as one initial state peak F_3 and two final state peaks H_3 and J_3 on W(111)/Ba. In addition, we present the calculations of the emission currents in FE and surface PFE, and of the surface electronic structures of W(110)/Ba (2×2) and W(111)/Ba (1×1). Our results account for the energies of all of the initial and final state features observed experimentally in FE, PFE, and photoemission.[14,15] We show that the TEDs in PFE from the atomically less dense overlayer W(110)/Ba (2×2) are dominated by substrate-overlayer interactions, while those from the atomically denser overlayer W(111)/Ba (1×1) are dominated by interactions within the overlayer. Our results yield evidence that with increasing Ba coverage above 1/3 ML on W(111) [corresponding to a commensurate $(3^{1/2}\times3^{1/2})R30°$ overlayer], the interstitial sites fill in randomly to form a commensurate (1×1) overlayer at 1 ML coverage.

In this paper, the experimentally observed emission peaks are labeled alphabetically and the emitting facet is denoted by a numerical subscript (1 denotes 100, 2 denotes 110, and 3 denotes 111). The calculated peaks are denoted by a prime. The experimental procedures are described in Sec. II, and details of the electronic structure calculations are reported in Sec. III. In Secs. IV–VI, the experimentally measured TEDs in PFE from W(100)/Ba, W(110)/Ba, and W(111)/Ba are presented and interpreted on the basis of the calculations. The Ba-induced reductions in the work functions are also discussed. The conclusions of this work are summarized in Sec. VII.

II. EXPERIMENTAL METHOD

A. Measurements of the total energy distribution of the field emission current

A tungsten tip (a fine tungsten wire with a hemispherical end form of radius approximately 0.1 μm) is mounted on a tungsten support loop and placed about 5 cm from a fluorescent screen inside an ultrahigh vacuum chamber (the main chamber) at a pressure of less than 2×10^{-10} Torr. When a positive potential of several kilovolts is applied to the screen, electrons are emitted from the tip by quantum mechanical tunneling. The field emitted electrons are accelerated toward the fluorescent screen where they impact to produce a magnified image of work function variations of the surface of the tip. To study emission from a single facet, the image of the selected facet is deflected electrostatically onto a probe hole located in the center of the screen, and the total energy distribution of the current density $j(E)$ (the derivative of the current per unit area with respect to the total energy E) of FE electrons passing through the probe hole is measured.

Prior to each measurement, the tip was cleaned by momentarily passing a current through the tungsten support loop, raising its temperature to white heat. A beam of atomic Ba was obtained by heating a small lump of metallic Ba, enclosed in a molybdenum insert, inside a Knudsen cell.[17] The Ba flux was measured by means of a quartz-crystal thickness monitor and deposited at room temperature. Details of the FE and PFE spectrometers[18,19] and the atomic deposition system[20–22] have been reported elsewhere.

B. Measurements of the total energy distribution of the photofield emission current

PFE involves excitation by photons with energy less than the surface plasmon energy. Two distinct excitation mechanisms, surface and bulk photoexcitation, are involved. Surface photoexcitation is predominant when the polarization vector of the incident light has an appreciable component normal to the emitting surface (p polarization). Photons couple strongly to electrons in the tails of the wave functions just outside the surface of the metal, in the region where the plasmon energy associated with the local electron density is equal to the photon energy. The final states in surface photoexcitation are a continuum of free-electron-like states of the vacuum, and hence, any features observed in the TED in surface photoexcitation correspond to the initial states of the

optical transitions. Bulk photoexcitation occurs when the polarization vector of the incident light is parallel to the emitting surface (*s* polarization). The incident photons enter the metal, where they induce direct (energy and crystal-momentum conserving) transitions from occupied to unoccupied electron states. Both initial states and final states are observed in bulk photoexcitation. They can be distinguished experimentally because initial states appear at a constant initial state energy $E-\hbar\omega$, and final states appear at a constant final state energy E, irrespective of the photon energy $\hbar\omega$. The transition rate for surface photoexcitation is typically much greater than that for bulk photoexcitation, and surface photoexcitation is more sensitive than bulk photoexcitation to occupied electron states at the surface. For these reasons, the present work is based largely on measurements of surface photoexcitation.

Relative to the Fermi level, the energy of the peak of the surface potential barrier is $U_{max}=\Phi-(e^3F/4\pi\varepsilon_0)^{1/2}$, where Φ is the work function of the emitting surface, e is the magnitude of the electronic charge, F is the magnitude of the applied electric field, and ε_0 is the permittivity of free space. Therefore, electrons in initial states with normal energy greater than $U_{max}-\hbar\omega$ can pass above the peak of the surface potential barrier and make a strong contribution to the TED in PFE. As the total energy increases above the threshold, electron states of progressively larger transverse wave vector contribute to the PFE current. Therefore, PFE is a $\boldsymbol{k}$-resolved process that is dominated by emission from electron states close to the center of the surface Brillouin zone (SBZ).

The electrons were photoexcited by the focused beam of a cw krypton-ion laser.[23] A half wave retarder was used to adjust the plane of polarization of the laser beam to maximize surface photoexcitation. The blue line (2.60 eV), the violet line (3.00 eV), and the UV line (3.54 eV) were used. For the various spectral lines, the power in the focal spot was in the range of 40–100 mW.

C. Measurements of the work function

To a very good approximation, a Fowler-Nordheim plot[24,25] of the FE current I, a plot of $\ln(I/V^2)$ against $(1/V)$, is a straight line from whose slope the ratio $\Phi^{3/2}/\beta$ can be determined, where Φ is the work function and β is the facet-dependent factor that relates the electric field strength at the emitting facet F to the tip-to-screen potential V ($F=\beta V$). In the present work, the value of β for the clean facet was deduced from the slope of the measured Fowler-Nordheim plot, taking the work function of the clean facet from the literature. The work function of the same facet with a Ba overlayer was deduced by comparing the slopes of the measured Fowler-Nordheim plots and assuming that β is independent of coverage. This is a reasonable assumption because at 1 ML coverage, the overlayer does not significantly affect the geometry of the end form of the tip.

For each of the low-index W facets, the Ba exposure that corresponds to the minimum work function was measured by means of a quartz-crystal thickness monitor. Assuming a linear relationship between coverage and exposure, and knowing the coverage that corresponds to the minimum work function from LEED experiments reported in the literature [1 ML on W(100), corresponding to a Ba $c(2\times2)$ overlayer, 0.38 ML on W(110), corresponding to a Ba (2×3) overlayer,[2] and 0.6 ML on W(111) (Ref. 6)], the coverage was calculated as a function of exposure.

Several authors[1,8,13,26] have concluded that the minimum in the work function of Ba on W(100) occurs at a coverage of 5.0×10^{14} atoms cm^{-2}, which corresponds to an ordered Ba $c(2\times2)$ overlayer. In the present work, we found that the minimum in the work function occurs at a Ba exposure of $6.2(5)\times10^{14}$ atoms cm^{-2}. The discrepancy between the measured exposure and the resulting coverage suggests either that not all of the atoms incident on the tip are adsorbed or that some of the adsorbed atoms subsequently migrate away from the W(100) facet. The latter possibility is supported by observations of the field emission pattern, which show that Ba atoms diffuse from regions of the tip that are directly exposed to the incident atomic beam to regions on the tip that are not directly exposed. Similar considerations apply to the W(110) and W(111) facets.

III. COMPUTATIONAL METHOD

A. Total energy distribution of the field emission current

The metal-adsorbate-vacuum interface is represented by a supercell whose electronic structure is calculated self-consistently by the FP-LAPW method based on density functional theory (DFT) using the WIEN2K software package.[27] Exchange and correlation are treated in the generalized-gradient approximation (GGA).[28] Relativistic corrections including the spin-orbit interaction are included in the calculation.

Inside the interface plane $z=z_0$, which represents the electrical surface of the metal, the applied electrostatic field is assumed to be fully screened out by the valence electrons, so the potential is the self-consistent potential of a half-plane of atoms. Outside the interface plane, the potential energy of the electron can be written

$$U(z)=U_0 \quad \text{for } z_0\leqslant z\leqslant z_c,$$

$$U(z)=(E_F+\Phi)-e^2/[16\pi\varepsilon_0(z-z_0)]-eF(z-z_0) \quad \text{for } z>z_c, \tag{1}$$

where E_F is the Fermi energy.

The interface plane was chosen to be sufficiently far from the surface plane (the plane of the outer layer of atoms) that the potential energy varies weakly in the interface plane, but sufficiently close that all of the electron states in the energy range over which the emission current is to be calculated have positive kinetic energies in the interface plane. We found that when these two conditions are satisfied, the distance between the surface plane and the interface plane is approximately one-half of the nearest neighbor distance. The cutoff plane ($z=z_c$) was chosen so that $U(z)$ is a continuous function of z. In this model, the shape of the surface potential barrier [Eq. (1)], and hence its transmission coefficient, is independent of the choice of z_0.

The potential energy in the interface plane has the translational symmetry of the surface layer. Because the potential energy varies only weakly in the interface plane, the wave function of wave vector $\mathbf{k}=(\mathbf{k}_\parallel,k_z)$ at point $\mathbf{r}=(\mathbf{r}_\parallel,z_0)$ can be expanded in plane waves of wave vector $(\mathbf{k}_\parallel+\mathbf{G}_\parallel)$:

$$\psi_{\mathbf{k}}(\mathbf{r})=\sum_{\mathbf{G}_\parallel} A_{\mathbf{k},\mathbf{G}_\parallel}\exp[i(\mathbf{k}_\parallel+\mathbf{G}_\parallel)\cdot\mathbf{r}], \tag{2}$$

where $A_{\mathbf{k},\mathbf{G}_\parallel}$ are the expansion coefficients and $\mathbf{G}_\parallel$ are the surface reciprocal lattice vectors. For an electron state of total energy E, the normal energy of the plane wave component of wave vector $(\mathbf{k}_\parallel+\mathbf{G}_\parallel)$ is

$$W_{\mathbf{k},\mathbf{G}_\parallel}=E-U_0-[\hbar^2/(2m)](\mathbf{k}_\parallel+\mathbf{G}_\parallel)^2, \tag{3}$$

where $\hbar$ is Planck's constant and m is the free-electron mass. The transmission coefficient of the surface potential barrier $D(W_{\mathbf{k}},\mathbf{G}_\parallel)$ decreases exponentially as the normal energy decreases, so the FE current is dominated by states that are close to the center of the SBZ ($\mathbf{k}_\parallel\approx 0$) and by the zero order ($\mathbf{G}_\parallel=0$) component in the plane wave expansion. In calculating the FE current, it is an excellent approximation to take the contributions of the higher order ($\mathbf{G}_\parallel\neq 0$) components in the plane wave expansion to be zero.[29] This is the approximation on which the present calculations are based.

The contribution of the electron state $\mathbf{k}$ to the $\mathbf{G}_\parallel=0$ component of the layer density of states (LDOS) in the interface plane can be written identically as $F_{\mathbf{k}}$ $\mathrm{SDOS}_{\mathbf{k}}(E)$, where $\mathrm{SDOS}_{\mathbf{k}}(E)$ is the contribution of state $\mathbf{k}$ to the SDOS including all higher order components, and the factor $F_{\mathbf{k}}$ is given by

$$F_{\mathbf{k}}\equiv A^*_{\mathbf{k},0}A_{\mathbf{k},0}\Bigg/\left(S^{-1}\left\langle\int\psi_{\mathbf{k}}(\mathbf{r})^*\psi_{\mathbf{k}}(\mathbf{r})d\mathbf{S}\right\rangle\right). \tag{4}$$

In Eq. (4), the numerator is the contribution of state $\mathbf{k}$ to the $\mathbf{G}_\parallel=0$ component of the LDOS in the interface plane, and the denominator is the contribution of state $\mathbf{k}$ to the SDOS. The angular brackets indicate that the integral in the denominator is to be averaged over the surface layer. The expansion coefficients $A_{\mathbf{k},0}$ in Eq. (4) can be calculated by evaluating the integral

$$A_{\mathbf{k},0}=S^{-1}\int\psi_{\mathbf{k}}(\mathbf{r})\exp(-i\mathbf{k}_\parallel\cdot\mathbf{r}_\parallel)d\mathbf{S}, \tag{5}$$

over one lattice cell of area S in the interface plane.

The FE current is dominated by the s-, pz-, and dz^2-like electron states, because for these symmetries the coefficients $A_{\mathbf{k},0}$ do not vanish at $\bar{\Gamma}$. The $px+py$-, $dxz+dyz$-, $d(x^2-y^2)$-, and dxy-like states make only a small contribution to FE, because at $\bar{\Gamma}$ their wave functions are antisymmetric within the lattice cell,[30] so their coefficients $A_{\mathbf{k},0}$ vanish.

The distributed WIEN2K subroutine TETRA can be used to calculate the surface density of states (SDOS) by dividing the Brillouin zone into a large number of tetrahedra of equal volume and evaluating

$$\mathrm{SDOS}(E)=\sum_\kappa\sum_i\mathrm{SDOS}_{\kappa,i}(E), \tag{6}$$

where the distribution $\mathrm{SDOS}_{\kappa,i}(E)$ is the contribution of band i in tetrahedron κ to the density of states in the surface layer for a single direction of electron spin.[31] It follows from Eq. (4) that the contribution of band i in tetrahedron κ to the $\mathbf{G}_\parallel=0$ component of the LDOS in the interface plane can be written $F_{\kappa,i}\mathrm{SDOS}_{\kappa,i}(E)$.

The subroutine TETRA was modified to yield the TED in FE:

$$j_S(E)=2ef(E)\sum_\kappa\sum_i F_{\kappa,i}\mathrm{SDOS}_{\kappa,i}(E)v(W_{\kappa,i})D(W_{\kappa,i}), \tag{7}$$

where e is the magnitude of the electron charge, $f(E)$ is the Fermi-Dirac distribution function, and the factor of 2 takes into account the spin degeneracy of the electron. The factor $F_{\kappa,i}$ was calculated from Eqs. (4) and (5) at the center of each tetrahedron, using non-spin-orbit wave functions to evaluate the integrals. The contribution of state (κ,i) to the SDOS in the surface layer was estimated by averaging the integral in the denominator of Eq. (4) over three equally spaced planes spanning the surface layer (the plane of the outer layer of atoms). For an electron state of total energy $E_{\kappa,i}$, the normal energy $W_{\kappa,i}$ of the $\mathbf{G}_\parallel=0$ component in the region $z_0\leqslant z\leqslant z_c$ is

$$W_{\kappa,i}=E_{\kappa,i}-U_0-\hbar^2\mathbf{k}_\parallel^2/(2m), \tag{8}$$

and the normal velocity with which the electrons approach the surface potential barrier is

$$v(W_{\kappa,j})=(2W_{\kappa,i}/m)^{1/2}. \tag{9}$$

To obtain the transmission coefficient of the surface potential barrier $D(W_{\kappa,i})$, the one-dimensional Schrödinger equation was solved numerically to evaluate the normal wave function across the surface potential barrier at normal energy $W_{\kappa,i}$ using an exact numerical technique due to Vigneron and Lambin.[32–34] Then $D(W_{\kappa,i})$ was calculated as the ratio of the charge fluxes on the two sides of the barrier as deduced from the Wronskian of the normal wave function.

The TED of the FE current calculated from Eq. (7) is denoted $j_S(E)$, where the subscript S denotes a surface contribution, because the present calculations are based on supercells that accurately model the surface layers of the metal but underrepresent the bulk. To make a direct comparison with the experimental data, $j_S(E)$ was corrected by adding $j_0(E)$, the bulk contribution estimated from the free-electron model.[35–37]

The TED in FE is dominated at low energy by the exponential decrease in the transmission coefficient of the surface potential barrier $D(W)$, and at high energy by the exponential decrease in the Fermi-Dirac distribution function $f(E)$, resulting in a peak at the Fermi energy. In analyzing the experimental data, it is convenient to remove the exponential energy dependencies below and above E_F by dividing the TED $j(E)$ by $j_0(E)$. The ratio $j(E)/j_0(E)$ is called the *enhancement factor*.

B. Total energy distribution of the photofield emission current

The subroutine TETRA was also modified to carry out FP-LAPW calculations of the TED in surface PFE. Schwartz and Cole[38] have shown that, apart from an energy-independent prefactor, the probability of surface photoexcitation from initial state $\boldsymbol{k}$ is given by $[W_{\boldsymbol{k}}(W_{\boldsymbol{k}}+\hbar\omega)]^{-1/2}|M|^2$, where M is an electric-field-dependent optical matrix element. They found that $|M|^2$ varies by only about 1% over the range of electric fields in the present experiments, and this small variation is neglected in the present calculations. The TED in surface PFE at final state energy E is obtained by evaluating the sum over tetrahedra κ and bands i:

$$j(E) \propto f(E-\hbar\omega)\sum_{\kappa}\sum_{i} F_{\kappa,i}\mathrm{SDOS}_{\kappa,i}(E-\hbar\omega) \times \frac{|M|^2}{[W_{\kappa,i}(W_{\kappa,i}+\hbar\omega)]^{1/2}} v(W_{\kappa,i}+\hbar\omega)D(W_{\kappa,i}+\hbar\omega), \tag{10}$$

where $f(E-\hbar\omega)$ is the Fermi-Dirac distribution function at the initial state energy $(E-\hbar\omega)$. The normal energy $W_{\kappa,i}$ of the $\mathbf{G}_{\parallel}=0$ component of the initial state is related to the total energy $E_{\kappa,i}$ of the initial state by Eq. (8), and $v(W_{\kappa,i}+\hbar\omega)$ can be calculated from Eq. (9). $F_{\kappa,i}$ was calculated as in Eq. (4), but the numerator was averaged over three equally spaced planes spanning the region just outside the surface plane where surface photoexcitation predominantly occurs. The interface plane plays no role in our PFE calculations. The transmission coefficient $D(W_{\kappa,i}+\hbar\omega)$ was evaluated numerically as described above.[32–34]

C. *k*-resolved layer density of states

Finally, the subroutine TETRA was modified to weight each contribution to the LDOS by the tunneling factor in field emission $D(W_{\kappa,i})$. The modified program yields the K-LDOS.

$$\text{K-LDOS}(E) = \sum_{\kappa}\sum_{i}\frac{\mathrm{LDOS}_{\kappa,i}(E)D(W_{\kappa,i})}{D(E)}. \tag{11}$$

While K-LDOS(E) is not an experimentally measurable quantity, a plot of K-LDOS(E) is a useful way to represent the energies and symmetries of features of the electronic structure in the vicinity of $\bar{\Gamma}$. The K-LDOS in the surface layer is denoted K-SDOS.

D. Structures of the W-Ba-vacuum interfaces

1. Ba c(2×2) overlayer on W(100) [W(100)/Ba c(2×2)]

In the present calculations, the geometry of the W(100)/Ba $c(2\times2)$ interface is described by a supercell that consists of 13 W layers stacked parallel to the (100) plane, surrounded on each side by a region of half that volume containing one Ba atom. Because the Ba overlayer is highly mobile and very weakly bound to the W substrate, it is not expected to modify significantly the normal spacing between the W layers. Therefore, the normal spacing between the W layers was taken from room-temperature lattice constant data for clean tungsten. The conventional lattice parameter of the body-centered-cubic cell is 3.17 Å.[39]

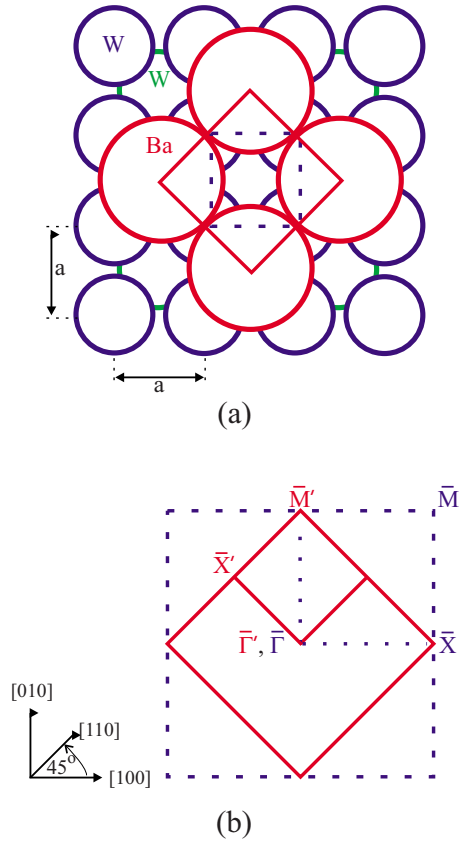

FIG. 1. (Color online) Surface unit cells and surface Brillouin zones of clean W(100) and of a Ba $c(2\times2)$ overlayer. (a) Atomic positions in the top two layers of W(100) and in the overlayer. Also shown are the primitive unit cells of the substrate (blue dashed lines) and of the overlayer (red solid lines). (b) The surface Brillouin zones of the substrate and of the overlayer plotted in the correct orientation relative to the unit cells in (a).

The calculated energy of the initial state peak F_1' in the TED in PFE, which corresponds to a prominent surface state of W(100)/Ba $c(2\times2)$, is very sensitive to the normal distance between the substrate and the overlayer. In an earlier self-consistent calculation,[16] a spacing of 2.49 Å was found to minimize the total energy of a five-W(100)-layer cell with a Ba layer on each side. Assuming this spacing, we calculated the energy of peak F_1' to be −1.50(2) eV, which does not compare well with the experimental energy of −1.90(5) eV. The present calculations are based on a normal distance of 2.77 Å, which we deduced from the published atomic radii of W and Ba.[39] The energy of peak F_1' [−1.80(2) eV] proved to be in much better agreement with experiment. Following the criteria stated in Sec. III A, the normal distance between the plane of the Ba overlayer and the interface plane was taken to be 2.16 Å.

In Fig. 1(a), the solid square represents a primitive unit cell of the Ba $c(2\times2)$ surface and the dashed square represents a primitive unit cell of the clean W(100) substrate. The corresponding SBZs are shown in Fig. 1(b). The symmetry

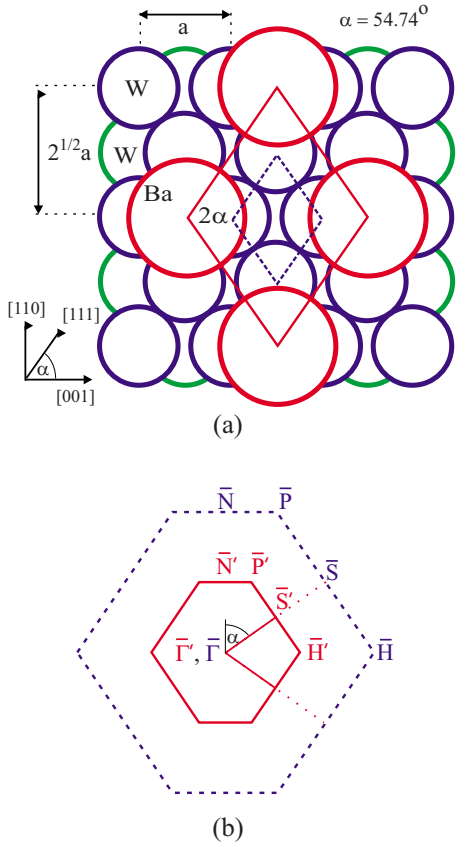

FIG. 2. (Color online) Surface unit cells and surface Brillouin zones of clean W(110) and of a Ba (2×2) overlayer. (a) Atomic positions in the top two layers of W(110) and in the Ba (2×2) overlayer. Also shown are the primitive unit cells of the clean substrate (blue dashed lines) and of the overlayer (red solid lines). (b) The surface Brillouin zones of the substrate and the overlayer plotted in the correct orientation relative to the unit cells in (a).

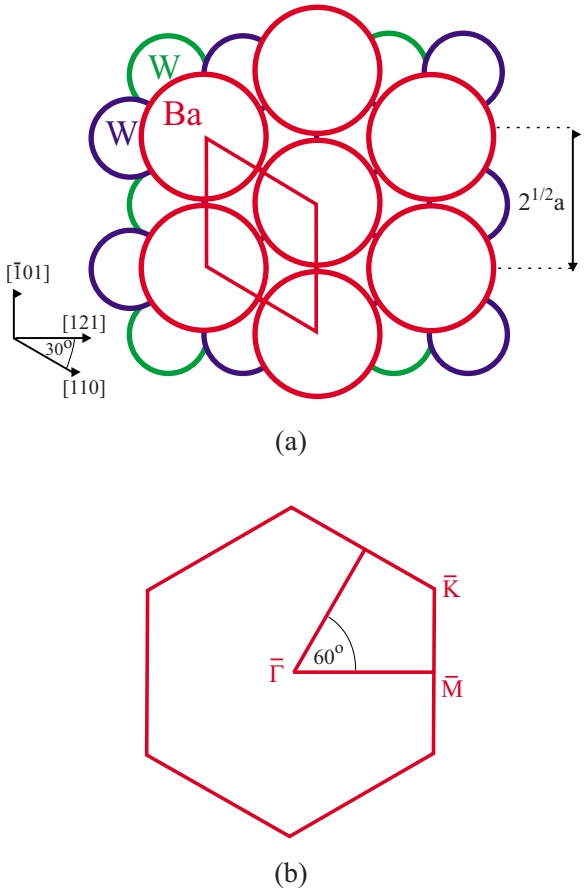

FIG. 3. (Color online) Surface unit cell and surface Brillouin zone of clean W(111) and of a Ba (1×1) overlayer. (a) Atomic positions in the top two hexagonal layers of W(111) and in the Ba (1×1) overlayer. Also shown is the primitive surface unit cell of the clean substrate and of the overlayer. (b) The surface Brillouin zone plotted in correct orientation with respect to the corresponding unit cell in (a).

points of the SBZ of the $c(2\times2)$ structure are denoted by a prime. The effect of the $c(2\times2)$ overlayer is to fold back the symmetry point $\bar{M}$ of the (1×1) substrate to $\bar{\Gamma}'$ in the SBZ of the overlayer.

2. Ba (2×2) overlayer on W(110) [W(110)/Ba c(2×2)]

The geometry of the W(110)/Ba (2×2) interface is represented by a supercell that consists of nine W layers stacked parallel to the (110) plane, surrounded on each side by a region of half that volume and containing one Ba atom. On the basis of the criteria stated above, the normal distance between the Ba overlayer and the W substrate was taken to be 3.19 Å, and the normal distance between the Ba overlayer and the interface plane was taken to be 2.11 Å.

In Fig. 2(a), the solid rhombus represents a primitive unit cell of the Ba (2×2) overlayer and the dashed rhombus represents a primitive unit cell of the clean W(110) substrate. The corresponding SBZs are shown in Fig. 2(b). The primes denote the symmetry points of the SBZ of the overlayer. The symmetry points $\bar{N}$ and $\bar{S}$ in the SBZ of the substrate are folded back to $\bar{\Gamma}'$ in the SBZ of the overlayer.

3. Ba (1×1) overlayer on W(111) [W(111)/Ba (1×1)]

The geometry of the W(111)/Ba (1×1) interface is represented by a supercell consisting of 19 W layers stacked parallel to the W(111) plane, surrounded on each side by a region of half that volume and containing one Ba atom. On the basis of the criteria stated above, the normal distance between the Ba overlayer and the W substrate was taken to be 2.44 Å, and the normal distance between the Ba overlayer and the interface plane was taken to be 2.01 Å.

In Fig. 3(a), the solid rhombus represents a primitive unit cell of the clean W(111) substrate and of the Ba (1×1) overlayer. The corresponding SBZ is shown in Fig. 3(b).

IV. RESULTS AND DISCUSSION FOR W(100)/Ba

A. Field and photofield emission currents

1. Experimental total energy distributions in field emission and photofield emission from W(100) with Ba overlayers

Our experimental TEDs in PFE from W(100), measured for Ba coverages in the range from 0 to 1 ML, are shown in

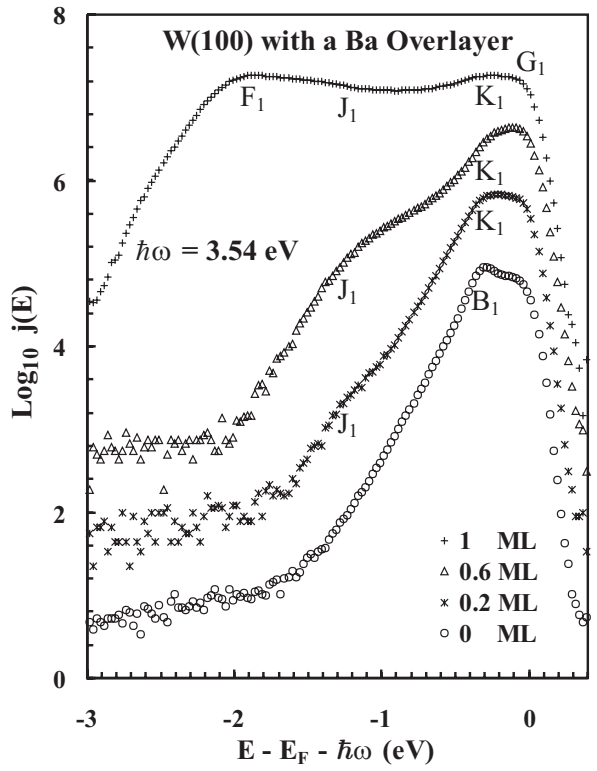

FIG. 4. Base 10 logarithms of the experimental TEDs in PFE with 3.54 eV photons for W(100)/Ba over a range of coverage, plotted as a function of the initial state energy $E-E_F-\hbar\omega$. The curves have been displaced vertically by arbitrary amounts for clarity.

Fig. 4. The electrons were excited by 3.54 eV photons in the focused *p*-polarized beam of a cw krypton-ion laser. The TED of the PFE current is plotted against the initial state energy $E-E_F-\hbar\omega$, where $E-E_F$ is the final state energy of the emitted electron relative to the Fermi level and $\hbar\omega$ is the photon energy. Increasing the Ba coverage reduces the work function, allowing electrons of progressively lower energy to tunnel through the surface potential barrier and shifting the low-energy cutoff in the TED to lower energy. Our corresponding TEDs using 2.60 and 3.00 eV photons have been reported elsewhere.[22] The energies of the experimental peaks measured relative to E_F are reported in Table I.

The TED in FE from clean W(100) shows a strong peak B_1 (the Swanson hump[40]) and a much weaker peak A_1.[30,41,42] These two peaks are suppressed by 0.1 ML coverage of Ba. The very strong initial state peak F_1 in the TED in PFE from W(100)/Ba is clearly resolved only at 1.0 ML coverage, where the final state energy is just above the peak of the surface potential barrier. Another initial state peak G_1 close to E_F is clearly resolved with 2.60 and 3.00 eV photons, but poorly resolved with 3.54 eV photons because it overlaps the final state peak K_1. In the range of coverage from 0.1 to 0.2 ML, our experimental FE data[22] also show a Ba-induced peak E_1 at about −0.08 eV (energies are expressed relative to E_F) that was detected by Radoń and Jaskólka[12] in PFE at less than 1 ML coverage.

The observed TEDs in PFE with 3.54 eV photons show two final state peaks K_1 and J_1 that appear at low Ba coverage and persist up to 1 ML. Our data with 2.60 and 3.00 eV photons also suggest the presence of a weak final state peak

TABLE I. Comparison of the experimentally observed peaks in the TEDs in FE and PFE from clean W(100) (A_1 and B_1) and W(100)/Ba $c(2\times2)$ (F_1–P_1), with peaks in the calculated TEDs and with bands observed in ARIPS. s.s. stands for surface states, s.r. for surface resonances, and bulk for bulk states.

Experiment			Calculated			
				Present work		
Peak label	Present work $E-E_F$ (eV)	ARIPS[a] $E-E_F$ (eV)	Peak label	$E-E_F$ (eV)	Character	Symmetry in overlayer [substrate]
A_1	−0.73(5)		A_1'	−0.69(2)	s.r.	$[dxz+dyz]$
B_1	−0.32(3)		B_1'	−0.32(2)	s.s	$[dz^2]$
F_1	−1.90(5)		F_1'	−1.80(2)	s.s.	s $[dz^2]$
G_1	Vicinity of 0.00(5)		G_1'	+0.14(2)	s.s.	$d(x^2-y^2)$ $[dz^2]$
H_1	+1.55(5)		H_1'	+1.55(2)	s.r.	dz^2 $[dz^2]$
J_1	+2.25(5)	+2.3 ($\bar{X}'$)	J_1'	+2.30(2)	s.r.	dz^2 $[dz^2]$
K_1	+3.25(5)		K_1'	+3.25(2)	bulk	dz^2 $[dz^2]$
			L_1'	−0.65(2)	s.s. ($\bar{X}'$)	$dxz+dyz$ $[dxz+dyz]$
			M_1'	+0.25(2)	s.s.	pz $[dz^2]$
N_1		+0.6 ($\bar{X}'$)	N_1'	+0.50(2) +0.65(2)	s.r. ($\bar{X}'$)	$dxz+dyz$ $[dz^2]$
P_1		+3.2 ($\bar{X}'$) to +3.6 ($\bar{\Gamma}'$)	P_1'	+3.20 to +3.65(2)	s.r. and bulk	$dxz+dyz$ $[dz^2, dxy]$

[a]References 1 and 13

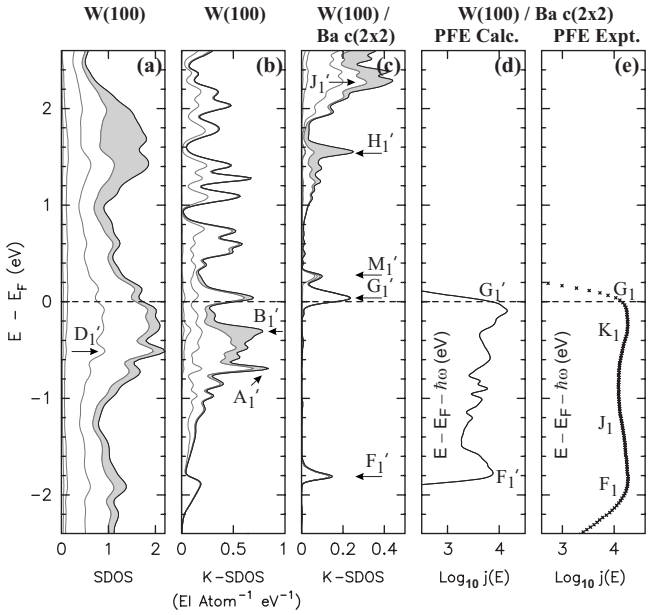

FIG. 5. (a) SDOS of clean W(100), (b) K-SDOS of clean W(100), and (c) K-SDOS of a Ba $c(2\times2)$ overlayer on W(100). (b) and (c) are plotted in the SBZ of the overlayer. The successive curves in the cumulative plots (a), (b), and (c) show the contributions of *s*-, *p*-, $dxy+d(x^2-y^2)$-, and $dxz+dyz$-, and dz^2-like states, respectively. The shading denotes the dz^2-like contributions. [(d) and (e)] TEDs in PFE for W(100)/Ba $c(2\times2)$ with 3.54 eV photons, plotted against the initial state energy. The calculated plot (d) is based on surface photoexcitation. The experimental plot (e) shows two additional final state peaks J_1 and K_1 that are attributed to bulk photoexcitation.

H_1 that is not resolved with 3.54 eV photons because it overlaps the strong initial state peak F_1.

2. *Interpretation of total energy distributions in field emission and photofield emission from* W(100)/Ba $c(2\times2)$

Electron states of clean W(100). Figures 5(a) and 5(b) show respectively the SDOS and the K-SDOS of clean W(100). The SDOS shows a region of strong surface-induced peaks that extends from −0.8 eV to just above E_F. Peak A_1' in the K-SDOS is responsible for the weak peak A_1 observed in the TED in FE from clean W(100), while peak B_1' is responsible for the observed strong peak B_1. In Table I, the calculated emission peaks from clean W(100) are compared with peaks observed in the present FE and PFE experiments (Sec. IV A 1), and their energies and symmetries are reported.

Electron states of an isolated Ba $c(2\times2)$ overlayer. The dispersion plot for an isolated Ba layer [Fig. 6(b)] was calculated using a supercell in which Ba atoms occupy the same sites as in the W(100)/Ba $c(2\times2)$ supercell and the W sites are empty. Along $\bar{\Gamma}'\bar{X}'$, the *s*-like valence states form a nearly-free-electron band. The bottom of the band is at −2.08 eV and the bandwidth along $\bar{\Gamma}'\bar{X}'$ is 1.40 eV. Above −0.68 eV, the valence states are predominantly *dxy*-like.

Occupied electron states of W(100)/Ba $c(2\times2)$. Figures 5(d) and 5(e) show respectively the base 10 logarithms of the

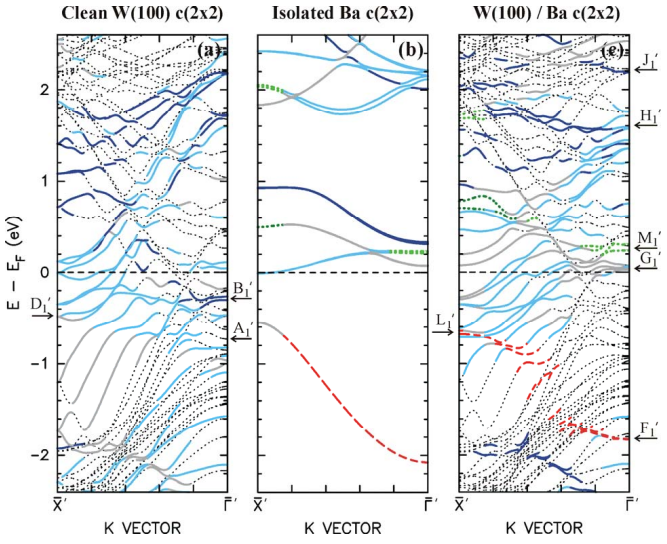

FIG. 6. (Color online) (a) Dispersion along $\bar{X}'\ \bar{\Gamma}'$ of (a) clean W(100), (b) an isolated Ba $c(2\times2)$ overlayer, and (c) W(100)/Ba $c(2\times2)$, all plotted in the SBZ of the overlayer. Surface states and surface resonances are shown by thick curves. The predominant symmetry in the surface layer is shown by the line style [*s*, red (dashed); *p*, green (dotted); and *d*, blue or gray (solid)]. Bulk and intermediate states are shown by thin gray (dotted) curves.

calculated and experimental TEDs of the PFE current from W(100)/Ba $c(2\times2)$ at room temperature, plotted against the initial state energy. In our calculations, the electrons were assumed to be excited by 3.54 eV photons in a *p*-polarized beam, the electric field strength was taken to be 0.11 V Å^{-1}, and the work function was taken to be 2.65 eV, as determined from the experimental data. The energy of the peak of the surface potential barrier is +1.42 eV (Sec. II B), so electrons in states having normal energy less than −2.12 eV will be photoexcited to states below the peak of the barrier. This accounts for the exponential cutoff in the TED in PFE below about −2.0 eV. In Table I, the calculated emission peaks from W(100)/Ba $c(2\times2)$ are compared with peaks observed at 1 ML Ba coverage in the present FE and PFE experiments (Sec. IV A 1) and in ARIPS at 1 ML Ba coverage,[1,13] and their energies and symmetries are reported.

When the interaction between the clean W(100) substrate and the Ba $c(2\times2)$ overlayer is turned on, the *s*-like states of the overlayer near $\bar{\Gamma}'$ [Fig. 6(b)] hybridize with the pair of surface states of the substrate at −0.27 and −0.30 eV [labeled B_1' in Fig. 6(a)], shifting them to F_1' at −1.82 eV [Fig. 6(c)]. Unoccupied *d*-and *p*-like states of the overlayer also hybridize with the same pair of surface states B_1' to yield surface states G_1' and M_1' just above E_F. Peak F_1 in the experimental TED in PFE at 1 ML Ba coverage [Fig. 5(e)] is attributed to the calculated peak F_1' [Fig. 5(d)], and peak G_1 is attributed to the low-energy tail of the calculated peak G_1'. Near $\bar{X}'$, the occupied *d*- and *s*-like states of the overlayer hybridize with the surface resonances D_1' of clean W(100) at −0.55 eV, shifting them to L_1' at −0.65 eV and yielding peak L_1' in the LDOS of W(100)/Ba $c(2\times2)$ [Figs. 7(d) and 7(e)].

The good overall agreement between the energies of the observed and calculated emission peaks in FE, PFE, and

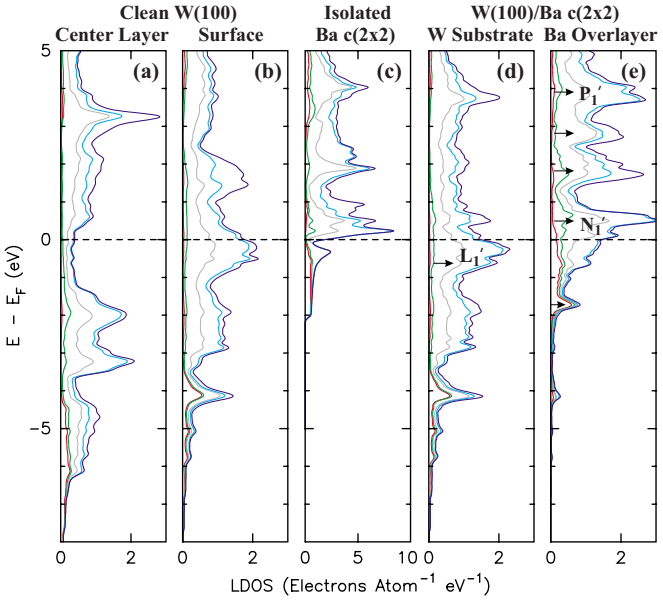

FIG. 7. (Color online) LDOS of clean W(100) in the (a) central (bulk) layer and (b) surface layer. (c) LDOS in an isolated Ba $c(2\times2)$ layer. LDOS of W(100)/Ba $c(2\times2)$ in (d) W substrate and (e) Ba overlayer. In these cumulative plots, the areas between successive curves show the contributions of *s*-like (red), *p*-like (green), $dxy+d(x^2-y^2)$-like (gray), $dxz+dyz$-like (light blue), and dz^2-like (dark blue) states, respectively.

ARIPS (Table I) indicates that the present calculations give a realistic picture of the electronic structure of the W(100)/Ba $c(2\times2)$ interface.

The instrumental resolution function of the energy analyzer used in the present experiments is of Gaussian form, with a full width at half maximum height of approximately 56 meV. Even after correcting for instrumental broadening by the energy analyzer, the peaks observed in the experimental TED in FE from clean W(100) are significantly wider than those in the calculated TED.[30] The additional broadening can be represented by a Lorentzian whose full width at half maximum height is proportional to the energy of the FE electrons relative to the Fermi level, and hence, to the total number of final states available for scattering. The absence of significant temperature dependence in the additional broadening of the Swanson peak over the range 78–300 K suggests that the additional broadening is predominantly lifetime broadening due to scattering by defects at the emitting surface. These conclusions are expected to apply also in the presence of an overlayer.

In early discussions of FE, it was assumed that the TED of the emission current is a measure of the K-SDOS. Taking into account the symmetries of the Bloch states, as in the present work, yields greatly improved results for the relative strengths of the calculated peaks in FE and surface PFE. Our results for clean W(100) suggest that the remaining discrepancies in the relative strengths of the emission peaks are dominated by lifetime broadening due to scattering by defects at the emitting surface. It seems likely that any additional discrepancies in the relative strengths of the peaks in surface PFE are due to our simplified treatment of the surface photoexcitation matrix element of Schwartz and Cole.[38]

Hemstreet and Chubb[16] used the full-potential LAPW method for thin films to calculate the electronic structure of a Ba $c(2\times2)$ overlayer on W(100), neglecting the spin-orbit interaction for the valence electrons. They represented the interface by five W(100) layers, with a Ba overlayer at each side at a distance of 2.48 Å from the plane of the substrate. We found that for satisfactory convergence of our surface electronic structure calculations, the supercell must have at least two intermediate layers in register with the surface and the bulk. This means that the supercell for clean W(100) should have a minimum of 13 W(100) layers. Therefore, the present calculations are expected to yield a more accurate description of the transition of the electronic structure of W(100)/Ba $c(2\times2)$ from the surface to the bulk than the earlier five layer calculations.

Hemstreet and Chubb[16] found, in agreement with the present results, that the *d*-like states of W hybridize with the *s*-like and *d*-like states of Ba, and that adsorbing a Ba $c(2\times2)$ overlayer on W(100) decreases the LDOS at the energy of the Swanson hump. However, while the present calculations show that the surface states that are responsible for the Swanson hump are shifted from −0.33 eV on clean W(100) to −1.80 eV on W(100)/Ba $c(2\times2)$, Hemstreet and Chubb did not report a similar shift.

Unoccupied electron states of W(100)/Ba $c(2\times2)$. In the present work, unoccupied electron states of W(100)/Ba $c(2\times2)$ are observed as final states in PFE. In the presence of a $c(2\times2)$ overlayer, the symmetry point $\bar{M}$ in the SBZ of clean W(100) is folded back to $\bar{\Gamma}'$ in the SBZ of the overlayer. Because FE and PFE are both dominated by emission from electron states close to $\bar{\Gamma}'$, states at $\bar{M}$ in the SBZ of the (1×1) W(100) substrate are expected to make a negligible contribution to emission from clean W(100) but a significant contribution to emission from W(100)/Ba $c(2\times2)$. This effect is responsible for the surface resonance band J_1' [Fig. 6(c)] and for the weak final state peak J_1 observed in PFE (Fig. 4).

The final state peak H_1 is attributed to peak H_1' in the K-SDOS [Fig. 5(c)], which is due to a high density of surface resonances close to $0.2\bar{\Gamma}'\bar{X}'$ [Fig. 6(c)]. The final state peak K_1 (Fig. 4) was observed in PFE with 3.54 eV photons over the whole range of Ba coverage. A similar peak was previously observed in PFE from clean W(100) using 3.54 eV *s*-polarized illumination.[18] These peaks are attributed to peak K_1' in the calculated K-LDOS that extends from the bulk layer to the layer beneath the substrate.

In summary, our calculations account for the energies of all of the well-resolved peaks observed experimentally in the TEDs in FE from clean W(100), as well as all of the peaks observed in PFE and in ARIPS from W(100)/Ba $c(2\times2)$ (Table I).

B. Layer density of states of clean W(100) and of W(100)/Ba $c(2\times2)$

1. Clean W(100)

The LDOSs in the central (bulk) layer and in the surface layer of the supercell of clean W(100) are shown in Figs.

7(a) and 7(b). Strong peaks in the SDOS [Fig. 7(b)] at about −4.1, −0.3, and +1.6 eV are suppressed in the bulk, while the strong bulk peak at about +3.2 eV [Fig. 7(a)] is suppressed at the surface. These differences are due to the breaking of translational symmetry and the reduced atomic coordination at the surface.

2. Isolated Ba layer

The LDOS of an isolated Ba layer, calculated using a supercell in which Ba atoms occupy the same sites as in the W(100)/Ba $c(2\times2)$ supercell and the W sites are empty, is shown in Fig. 7(c). The LDOS is predominantly *s*-like from −2.2 to −0.7 eV, and predominantly *dxy*-like from −0.7 eV to E_F.

3. W(100)/Ba $c(2\times2)$

The LDOSs in the substrate and in the overlayer of the supercell of W(100)/Ba $c(2\times2)$ are shown in Figs. 7(d) and 7(e). The strong peaks in the SDOS of clean W(100) at about −4.1 and −0.3 eV extend into the overlayer, while the strong peak in the SDOS of clean W(100) at +1.6 eV is suppressed in the substrate and the overlayer. Several additional surface resonance peaks appear in the overlayer [arrows in Fig. 7(e)]. Some of the calculated peaks are consistent with peaks that have been observed experimentally by Lamouri *et al.*[1,13] using ARIPS, as shown in Table I.

A band observed by Lamouri *et al.* in ARIPS,[1,13] having an energy of about +0.6 eV at $\bar{X}'$ and dispersing very little along $\bar{X}'\bar{\Gamma}'$, is consistent with the overlapping surface resonance peaks N_1' in the SDOS of W(100)/Ba $c(2\times2)$ [Fig. 7(e)]. They reported two weak surface state peaks in ARIPS at +2.3 and +2.7 eV that originate from electron states close to $\bar{M}'$ and close to $0.5\bar{\Gamma}'\bar{M}'$, respectively. It seems likely that the calculated peak in the SDOS at +2.7 eV is responsible for the higher energy ARIPS peak. They also observed a band that disperses from +3.6 eV at $\bar{\Gamma}'$ to +3.2 eV at $\bar{X}'$, which they interpreted as being due to a combination of Ba-induced states and W bulk states. It is likely that the strong peak P_1' in the calculated LDOS corresponds to electron states in the band observed in ARIPS.

Nonmetal-to-metal transitions in overlayers of divalent atoms on transition metal surfaces have been studied by several authors.[43,44] Plummer and Dowben[45] have shown that they involve a Wilson-like transition, in which the overlap between adjacent atomic orbitals causes the bandwidths to increase with increasing atomic density, until eventually band overlap results in metallic behavior. Electronic structure calculations for isolated layers of the alkaline earths Be, Mg, Ca, Sr, and Ba have been carried out by Yakovkin[46] for hexagonal structures of varying atomic density. At low atomic density, there is a gap between the occupied and unoccupied bands, resulting in a nonmetallic layer, while at higher atomic density, the gap disappears and the layer becomes metallic.

An isolated hexagonal Ba layer is nonmetallic at a lattice constant of 5.8 Å, but is metallic at a lattice constant of 4.3 Å.[46] The atomic density in the Ba $c(2\times2)$ layer (0.05 atom $Å^{-2}$) is intermediate between these two cases. We find that an isolated Ba $c(2\times2)$ layer is weakly metallic, having a small SDOS at E_F [Fig. 7(c)], and that interaction with the W substrate greatly increases the SDOS at E_F and, hence, the metallicity of the overlayer [Fig. 7(e)].

We found that if the muffin-tin radius is large enough, the total charge of 1.95 electrons within the muffin-tin sphere of Ba does not change significantly upon adsorption (in the present calculation, the muffin-tin radius for Ba was taken to be 2.1 Å). Instead, the total charge is redistributed among the various symmetry components. The *s*-like charge (integrated LDOS) decreases by about 0.34 electrons per Ba atom, and the *p*-like and *d*-like charges increase correspondingly. This is in contrast to the results of Hemstreet and Chubb,[16] who reported that the total charge inside the muffin-tin sphere of Ba increases significantly when the Ba is adsorbed on W(100), although they did not report the muffin-tin radius they used. They argued that the charge increases because the localized W surface states and resonances are attracted toward the Ba nuclei.

C. Effect of Ba adsorption on the work function of W(100)

1. Experimentally observed decrease of the work function

It is well established that the work function of W(100)/Ba decreases to a broad minimum at 1 ML coverage,[1,3,47] and that the magnitude of the decrease depends on the thermal history of the overlayer. In the present work, the work function at room temperature was found to decrease from 4.6 eV for clean[37,41,48] W(100) to 2.6 eV for a 1 ML unannealed overlayer. The maximum decrease of 2.0(2) eV is close to the maximum decrease of 2.3 eV found by Schmidt[47] for a 1 ML annealed overlayer at 78 K by the same method, and is close to the maximum decrease of 2.0 eV found by Lamouri and Krainsky[1] by the retarding field method.

2. Calculated Ba-induced charge shifts and surface electric dipole layers

Typically, valence electrons spill out from the surface of a clean transition metal, producing an inwardly directed surface electric dipole layer that increases the work function. Alkali and alkaline-earth overlayers on transition metal surfaces produce additional surface electric dipole layers whose net effect is to decrease the work function.

The spatial redistribution of the valence electron density that occurs when a Ba $c(2\times2)$ overlayer is adsorbed on W(100) was calculated by subtracting the sum of the valence electron density distribution of the clean W substrate and of the isolated Ba $c(2\times2)$ overlayer from the valence electron density distribution of W(100)/Ba $c(2\times2)$. The redistribution of the electron density in a {110} plane that passes through the metal surface is shown in Fig. 8. The most prominent features are a strong outwardly directed surface electric dipole layer in the region between the substrate and the overlayer, and a weak inwardly directed electric dipole layer just outside the surface layer. The net effect of these Ba-induced surface dipole layers is to decrease the work function.

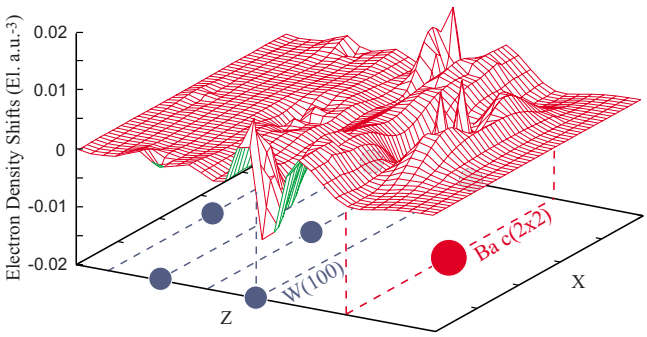

FIG. 8. (Color online) Calculated redistribution of the valence electron density that occurs when a Ba $c(2\times2)$ overlayer is adsorbed on a W(100) surface, plotted in a {110} plane that intersects the surface at right angles. The dashed rectangles represent the planes of the overlayer (labeled Ba) and of the substrate (labeled W). A positive shift corresponds to an increase in electron density.

The work function of W(100)/Ba $c(2\times2)$ was estimated by calculating the difference between the Coulomb potential energy far into the vacuum region of the supercell and the Fermi energy. According to the present calculation, the adsorption of a Ba $c(2\times2)$ overlayer on W(100) decreases the work function by 2.0(1) eV. This result is in good agreement with the decrease of 2.0(2) eV observed experimentally in the present work, and with the result of a full-potential LAPW calculation by Hemstreet and Chubb,[16] who found that a 1 ML Ba overlayer decreases the work function of W(100) by 1.9 eV. Because changes in the work function are dominated by charge shifts in the first two layers of the lattice, it is not surprising that the five layer calculation of Hemstreet and Chubb and the present 13 layer calculation yield very similar results.

V. RESULTS AND DISCUSSION FOR W(110)/Ba

A. Field and photofield emission currents

1. Experimental total energy distributions in field emission and photofield emission from W(110) with Ba overlayers

In Fig. 9, our experimental TEDs in PFE from W(110) for Ba coverages in the range from 0 to 0.6 ML are plotted against the initial state energy $E-E_F-\hbar\omega$. The electrons are excited by 3.54 eV photons in a focused p-polarized laser beam. With increasing Ba coverage, the work function of W(110)/Ba decreases to a minimum at 0.4 ML, enabling electrons of progressively lower energy to tunnel through the surface potential barrier and shifting the low-energy cutoff in the TED to lower energy. Our TEDs in PFE with 2.60 and 3.00 eV photons are presented elsewhere.[22]

The experimental TEDs in PFE show several peaks, whose energies are listed in Table II. A prominent initial state peak F_2 appears close to the low-energy cutoff even at the coverage of 0.4 ML that corresponds to the minimum in the work function. The strong energy dependence of the emission current in this energy range increases the uncertainty in determining the energy of peak F_2 from the experimental data. With as little as 0.02 ML of adsorbed Ba, the TEDs in

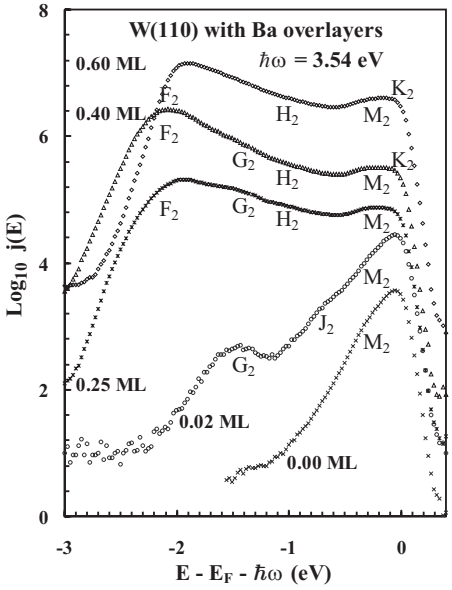

FIG. 9. Base 10 logarithms of the experimental TEDs in PFE with 3.54 eV photons for W(110)/Ba over a range of coverage, plotted as a function of the initial state energy $E-E_F-\hbar\omega$. The curves have been displaced vertically by arbitrary amounts for clarity.

PFE show two additional initial state peaks G_2 and J_2. Peak J_2 shifts from −0.68 eV at very low coverage to −0.72 eV at 0.60 ML coverage. In the range of coverage from 0.1 to 0.6 ML, the TEDs in PFE also show an initial state peak H_2, as well as enhanced emission, labeled K_2, close to E_F. The final state peak M_2 in the TEDs in PFE with 3.54 eV photons appears both for clean W(110) and for W(110)/Ba over the whole range of coverage. Because no corresponding peak appears at the same initial state energy in PFE with 2.60 and 3.00 eV photons, peak M_2 is interpreted as being a final state peak.

Our experimental TEDs in FE from W(110) for Ba coverages in the range from 0 to 1 ML have been reported elsewhere.[22] At coverages greater than 0.30 ML, they show a peak L_2 just above E_F. The exponential decrease in the FE current with energy above E_F increases the uncertainty in determining the energy of peak L_2 from the experimental data.

2. Interpretation of total energy distributions in field emission and photofield emission from W(110)/Ba (2×2)

Occupied electron states of W(110)/Ba (2×2). The calculated TEDs in FE and PFE from clean[22] W(110) are consistent with the experimental TEDs at 78 K (Ref. 41) and at room temperature[22] in that they show little structure over the energy range from −1.70 to +0.30 eV. The calculated K-SDOS and the base 10 logarithms of the calculated and experimental TEDs of the PFE current from W(110)/Ba (2×2) at room temperature, plotted against the initial state energy, are shown in Figs. 10(b)–10(d), respectively. The electrons were excited by 3.54 eV photons in a p-polarized beam. In our calculations, the electric field strength was

TABLE II. Comparison between the energies of peaks observed in the TEDs in FE and PFE from W(110)/Ba at 0.6 ML coverage and peaks observed in photoemission (Refs. 14 and 15) and PFE (Ref. 12), and the energies of the calculated peaks of W(110)/Ba (2×2). s.r. stands for surface resonances, bulk for bulk states, and int. for intermediate states (states having both surface and bulk characters).

Experiment				Calculated			
				Present work			
Peak label	Present work $E-E_F$ (eV)	Photoemission $E-E_F$ (eV)	PFE $E-E_F$ (eV)	Peak label	$E-E_F$ (eV)	Character	Symmetry in overlayer [substrate]
F_2	⩽−2.1	−2.2		F_2'	−2.10(2)	s.r.	s [dxz, dyz, $d(x^2-y^2)$]
G_2	−1.45(5)	−1.63		G_2'	−1.28(2)	int.	s, dyz [dz^2]
H_2	−1.05(5)	−1.01		H_2'	−1.02(2)	s.r.	s [dxz, dyz]
J_2	−0.72(5)	−0.54		J_2'	−0.61(2)	s.r.	s [dyz, $d(x^2-y^2)$]
		−0.54	−0.28(4)	N_2'	−0.45(2)	s.r.	dz^2 [p_z, $d(x^2-y^2)$]
K_2	Close to 0.0		−0.07(2)	K_2'	−0.08(2)	s.r.	dxz,dyz, [dxz,dyz]
L_2	⩾+0.1			L_2'	+0.35(5)	s.r.	d, p [d, p]
M_2	+3.25(5)			M_2'	+3.20(1)	bulk	dyz, dxy [dz^2, dxy]

taken to be 0.12 V Å^{-1} and the work function was taken to be 2.60 eV, as determined from the experimental data. The energy of the peak of the surface potential barrier is +1.32 eV, so only electrons having normal energy greater than −2.22 eV can pass above the peak of the barrier. In Table II, the energies and symmetries of the calculated peaks in the surface electronic structure of W(110)/Ba (2×2) are listed and the calculated peaks are compared with those observed in the present FE and PFE experiments at 0.6 ML Ba coverage, as well as with peaks observed in normal emission synchrotron radiation photoemission[14,15] at 0.6 ML Ba coverage and with PFE results[12] at less than 1 ML Ba coverage.

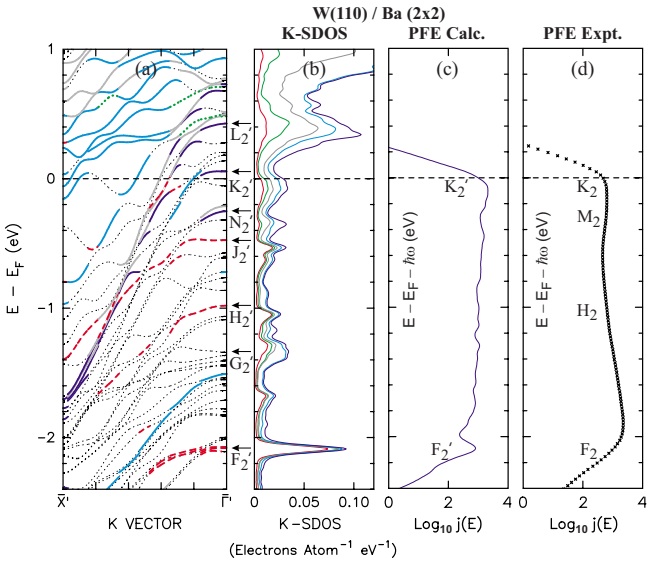

FIG. 10. (Color online) (a) Dispersion plots along $\bar{X}'$ $\bar{\Gamma}'$ in the surface Brillouin zone of W(110)/Ba (2×2). Surface states and surface resonances are shown by thick curves. The predominant symmetry in the surface layer is shown by the line style [s, red (dashed); p, green (dotted); and d, blue or gray (solid)]. Bulk and intermediate states are shown by thin gray dotted curves. (b) K-SDOS of W(110)/Ba (2×2). The successive curves in the cumulative plots show the contributions of s-, p-, $dxy+d(x^2-y^2)$-, $dxz+dyz$-, and dz^2-like, states respectively. [(c) and (d)] TEDs in PFE for W(110)/Ba (2×2) with 3.54 eV photons, plotted against the initial state energy. The calculated plot (c) is based on surface photoexcitation. The experimental plot (d) shows an additional final state peak M_2 that is attricuted to bulk photoexcition.

The strong peak F_2' in the calculated TED in PFE from W(110)/Ba (2×2) [Fig. 10(c)] is due to two Ba-induced bands of surface resonances close to $\bar{\Gamma}'$ [Fig. 10(a)]. The initial state peak F_2 in the experimental TED in PFE at 0.6 ML Ba coverage [Fig. 10(d)] is attributed to the calculated peak F_2'. The broad peak G_2' in the K-SDOS of W(110)/Ba (2×2) [Fig. 10(b)] is due to two bands of intermediate states. Peaks J_2', K_2', and N_2' in the K-SDOS are all due to Ba-induced bands of surface resonances. In the presence of a (2×2) overlayer, the symmetry point $\bar{S}$ in the SBZ of clean W(110) is folded back to $\bar{\Gamma}'$ in the SBZ of the overlayer. Because FE and PFE are dominated by emission from electron states close to $\bar{\Gamma}'$, states at $\bar{S}$ in the SBZ of the substrate are expected to make a negligible contribution to FE from clean W(110) but a significant contribution to FE from W(110)/Ba (2×2). This effect is responsible for the surface resonance band that yields peak H_2' in the K-SDOS. The initial state peaks G_2, H_2, J_2, and K_2, in the experimental TEDs in PFE (Fig. 9) are attributed to the calculated peaks G_2', H_2', J_2', and K_2', respectively.

Pi *et al.*[14,15] observed strong surface state peaks in synchrotron radiation photoemission at normal emission from clean W(110) at −1.41, −0.95, and −0.41 eV. These peaks were found to lose strength and to shift to −1.63, −1.01, and −0.54 eV, respectively, at 0.6 ML coverage. They most likely correspond to peaks G_2', H_2', and (J_2' or N_2') in Table II, respectively. Pi *et al.* also observed a peak that shifts from −2.0 eV for clean W(110) to −2.2 eV at 0.60 ML coverage, which they attributed to electrons embedded between the top

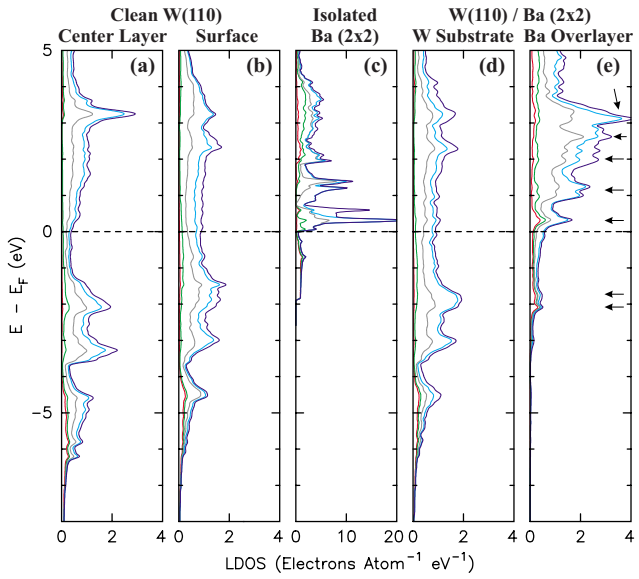

FIG. 11. (Color online) LDOS of clean W(110) in the (a) central (bulk) layer and (b) surface layer. (c) LDOS in an isolated Ba (2 ×2) layer. LDOS of W(110)/Ba (2×2) in (d) W substrate and (e) Ba overlayer. In these cumulative plots, the areas between successive curves show the contributions of *s*-like (red), *p*-like (green), $dxy+d(x^2-y^2)$-like (gray), *dxz*+*dyz*-like (light blue), and dz^2-like (dark blue) states, respectively.

surface and the second layer. This peak is attributed to the calculated peak F_2'.

Radoń and Jaskólka,[12] using 1.96 and 2.54 eV photons, found enhanced PFE from W(110)/Ba at −0.07(2) eV and at −0.28(4) eV with less than 1 ML coverage. The peak at −0.07 eV corresponds to the calculated peak K_2', while the peak at −0.28 eV may correspond to the calculated peak N_2'. Peak N_2' may also correspond to a broad peak at −0.41 eV that was detected by Plummer and Young[10] in FE from Ba atoms singly adsorbed on W(110).

Unoccupied electron states of W(110)/Ba (2×2). Several superimposed peaks L_2' in the K-SDOS of W(110)/Ba (2×2) [Fig. 10(b)] are due to a group of closely spaced surface resonance bands [Fig. 10(a)]. Peak L_2, just above E_F in the experimental TED in FE,[22] is attributed to these bands. The final state peak M_2 in the experimental TEDs in PFE (Fig. 9) was observed with 3.54 eV photons both for clean W(110) and for W(110) with Ba overlayers over the whole range of coverage. The experimental peak M_2 is attributed to emission from bulk states M_2' of clean W(110) that extend into the surface and overlayer, respectively.

In summary, our calculations account for the energies of all of the peaks observed in PFE and photoemission from W(110)/Ba (2×2) (Table II).

B. Layer density of states of clean W(110) and of W(110)/Ba (2×2)

1. Clean W(110)

Prominent peaks in the bulk LDOS at −3.3 and +3.2 eV [Fig. 11(a)] are greatly attenuated in the surface layer of clean W(110) [Fig. 11(b)], while prominent surface peaks appear at −3.0, −1.5, and +2.3 eV, which grow progressively weaker in the subsurface layers. These differences are a consequence of the breaking of translational symmetry and the reduced atomic coordination at the surface.

2. Isolated Ba (2×2) layer

The LDOS of an isolated Ba layer, calculated using a supercell in which Ba atoms occupy the same sites as in the W(110)/Ba (2×2) supercell and the W sites are empty, is shown in Fig. 11(c). The LDOS is predominantly *s*-like below −0.8 eV and predominantly $d(x^2-y^2)$-like above.

3. W(110)/Ba (2×2)

When the interaction between the substrate and the overlayer is turned on, the surface resonance peak of clean W(110) at −1.5 eV is suppressed [Fig. 11(d)], those at −3.0 eV and at +2.3 eV extend into the overlayer [Fig. 11(e)], and several additional Ba-induced surface resonance peaks appear [arrows in Fig. 11(e)].

Electronic structure calculations[46] for an isolated hexagonal Ba layer show that at low atomic density there is little overlap between the *s*- and *d*, *p*-like valence bands, and hence, weak metallicity. An isolated hexagonal Ba layer is found to undergo a metal-to-nonmetal transition at a lattice constant of 5.7 Å, which corresponds to an atomic density of 0.036 atom $Å^{-2}$. At E_F, the LDOS of an isolated Ba (2×2) layer of atomic density 0.035 atom $Å^{-2}$ is weak [Fig. 11(c)]. Interaction with the W(110) substrate greatly increases the LDOS at E_F, and hence, the metallicity of the overlayer [Fig. 11(e)].

C. Work function of W(110)/Ba (2×2)

According to the present calculation, the work function of W(110)/Ba (2×2) is less than that of clean W(110) by 2.6(2) eV. This is in good agreement with the experimental decrease of 2.6(2) eV for W(110)/Ba (2×2) deduced from a Fowler-Nordheim plot[24] of our FE data[22] for an overlayer at room temperature without prior annealing. It is clear from the literature[2–5,9,14,47] that the decrease in the work function of W(110) due to adsorbed Ba depends on the heat treatment of the field emitter. For overlayers at room temperature without prior annealing, the reported decreases in the work function at 0.6 ML coverage are 2.1 eV (Ref. 3) and 2.9 eV.[14]

VI. RESULTS AND DISCUSSION FOR W(111)/Ba

A. Field and photofield emission currents

1. Experimental total energy distributions in field emission and photofield emission from W(111) with Ba overlayers

In Fig. 12, our experimental TEDs in PFE from W(111)/Ba in the range of coverage from 0 to 1.0 ML are plotted against the initial state energy $E-E_F-\hbar\omega$. The electrons are excited by 3.54 eV photons in a focused *p*-polarized cw laser beam. Our experimental TEDs in PFE with photon energies 2.60 and 3.00 eV and in FE from

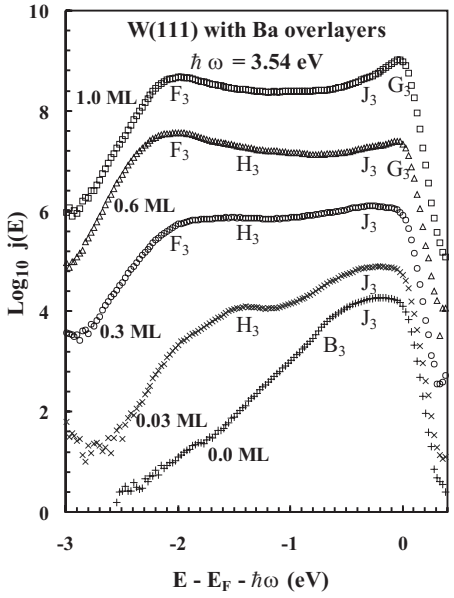

FIG. 12. Base 10 logarithms of the experimental TEDs in PFE with 3.54 eV photons for W(111)/Ba over a range of coverage, plotted as a function of the initial state energy $E-E_F-\hbar\omega$. The curves have been displaced vertically by arbitrary amounts for clarity.

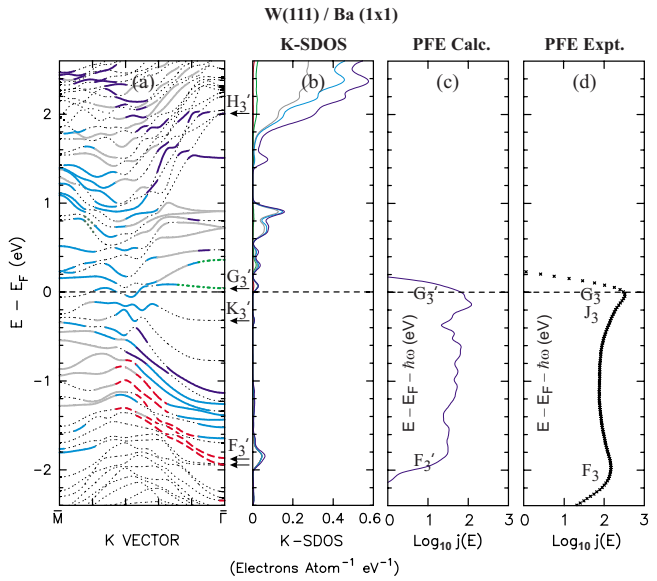

FIG. 13. (Color online) (a) Dispersion plots along $\bar{M}\ \bar{\Gamma}$ in the surface Brillouin zone of W(111)/Ba (1×1). Surface states and surface resonances are shown by thick curves. The predominant symmetry in the surface layer is shown by the line style [*s*, red (dashed); *p*, green (dotted); and *d*, blue or gray (solid)]. Bulk and intermediate states are shown by thin gray dotted lines. (b) K-SDOS of W(111)/Ba (1×1). The successive curves in the cumulative plots show the contributions of *s*-, *p*-, $dxy+d(x^2-y^2)$, $dxz+dyz$-, and dz^2-like states, respectively. [(c) and (d)] TEDs in PFE for W(111)/Ba (1×1) with 3.54 eV photons, plotted against the initial state energy. The calculated plot (c) is based on surface photoexcitation. The experimental plot (d) shows an additional final state peak J_3 that is attributed to bulk photoexcitation.

W(111) with Ba coverages in the range from 0 to 1 ML have been reported elsewhere.[22]

FE measurements from clean W(111) at 78 K (Ref. 41) show a strong asymmetrical peak with maximum emission at −0.75 eV as well as a broad peak centered at about −1.4 eV. The TEDs in PFE from clean W(111) at room temperature (the lowest curve in Fig. 12) and the enhancement factor[22] both show a similar asymmetrical peak B_3 that is suppressed by as little as 0.03 ML of Ba (Fig. 12). The rise in the experimental enhancement factor of clean W(111) just above E_F (Ref. 22) suggests the presence of a peak D_3. The exponential decrease in the FE current above E_F increases the uncertainty in determining the energy of peak D_3 from the experimental data. Peak D_3 in the TEDs in FE loses strength with increasing Ba coverage and cannot be detected above 0.4 ML.

Close to the minimum in the work function at 0.6 ML coverage, the TEDs in PFE show a strong rise in electron emission at about −2.0 eV that is interpreted as being an initial state peak F_3. Above 0.3 ML coverage, another initial state peak G_3 appears just above E_F.

The TEDs in PFE with 3.54 eV photons also show two final state peaks H_3 and J_3. Peak H_3 is observed in the range of coverage from 0.03 to 0.60 ML. Peak J_3 is observed in the TEDs from clean W(111) and from W(111)/Ba over the whole range of coverage. A region of high density of bulk states in this same energy range is responsible for peak K_1 in PFE from clean and Ba covered W(100) (Sec. IV A) and for peak M_2 in clean and Ba covered W(110) (Sec. V A).

2. *Interpretation of the total energy distributions in field emission and photofield emission from* W(111)/Ba (1×1)

Occupied electron states of W(111)/Ba (1×1). Our calculations for clean[22] W(111) show two bands of surface resonances of dz^2 symmetry that originate at $\bar{\Gamma}$ at about −0.57 and −0.42 eV, respectively, and disperse toward higher energy along $\bar{\Gamma}\bar{M}$. Emission from strongly lifetime broadened states B_3' in these bands may be responsible for the highly asymmetrical peak B_3 observed in FE and PFE (Fig. 12). Another band of intermediate states of predominantly dz^2-like symmetry that originates at $\bar{\Gamma}$ at +0.18 eV and disperses toward higher energy along $\bar{\Gamma}\bar{M}$ yields another asymmetrical peak D_3' at +0.18 eV. The rise in the experimental enhancement factor above E_F is consistent with emission from these states. Several bands of surface resonances close to $\bar{\Gamma}$ yield a weak peak A_3' in FE. Peak A_3' with strong lifetime broadening may account for the broad peak that appears in the 78 K data at about −1.4 eV.[41]

Figures 13(c) and 13(d) show, respectively, the base 10 logarithms of the calculated and experimental TEDs of the PFE current from W(111)/Ba (1×1) at room temperature. The electrons were excited by 3.54 eV photons. The electric field strength assumed in the calculations was 0.09 V Å^{-1} and the work function was 2.50 eV, as determined from the experimental data. The energy of the peak of the surface potential barrier is +1.49 eV, so only electrons in states having normal energy greater than −2.05 eV can pass above the peak of the barrier. This accounts for the cutoff in the TED in PFE below about −2.0 eV. In Table III, the calculated emis-

TABLE III. Comparison between the energies of the peaks observed in the TEDs in FE and PFE from clean W(111) (A_3–D_3) and W(111)/Ba at 1 ML coverage and FE (Ref. 41) and PFE (Ref. 12) results (F_3–K_3), and the energies of the calculated peaks of clean W(111) and W(111)/Ba (1×1). s.r. stands for surface resonances, bulk for bulk states, and int. for intermediate states.

Experiment			Calculated			
			Present work			
Peak label	Present work $E-E_F$ (eV)	FE and PFE $E-E_F$ (eV)	Peak label	$E-E_F$ (eV)	Character	Symmetry in overlayer [substrate]
A_3		−1.4(2)	A_3'	−1.30(2)	s.r.	$[d(x^2-y^2)+dxy, dxz+dyz, dz^2]$
B_3	−0.65(5)	−0.75(5)	B_3'	−0.57(2) −0.42(2)	s.r.	$[dz^2]$
D_3	+0.2(1)		D_3'	+0.18(2)	int.	$[dz^2]$
F_3	−2.0(1)		F_3'	−1.90(2)	s.r.	s $[dz^2]$
G_3	Close to 0.0	−0.07(2)	G_3'	+0.07(2)	s.r.	pz $[dz^2]$
H_3	+2.15(5)		H_3'	+2.05(2)	s.r.	dz^2 $[dz^2]$
J_3	+3.25(5)		J_3'	+3.33(2)	bulk	$d(x^2-y^2)+dxy$ and $dxz+dyz$
		−0.28(4)	K_3'	−0.32(2)	int.	s $[dz^2]$

sion peaks for W(111)/Ba (1×1) are compared with peaks observed at 1 ML Ba coverage in the present FE and PFE experiments, and the energies and symmetries of the calculated peaks are reported.

Hybridization with *s*-like states of the Ba (1×1) overlayer shifts the dz^2-like surface resonance bands of clean W(111) at −0.57 and −0.42 eV to F_3' at −1.94 and −1.86 eV, respectively [Fig. 13(a)]. The prominent peak F_3 in the experimental TEDs in PFE [Fig. 13(d)] is attributed to the calculated peak F_3' [Fig. 13(c)]. The unoccupied bands of dz^2-like surface resonances of clean W(111) at +0.18 and +0.58 eV are shifted to K_3' at −0.32 eV and to G_3' at +0.05 eV, respectively, by hybridization with *s*- and *p*-like states of the Ba (1×1) overlayer. Peak G_3 in the experimental TEDs in PFE is attributed to the calculated peak G_3'.

Radoń and Jaskólka[12] have measured PFE from W(111) with 1.96 and 2.54 eV photons at less than 1 ML coverage. They observed initial state peaks at −0.07(2) eV and at −0.28(4) eV, which they interpreted as being due to excitations of electrons in the Ba layer. Plummer and Young[10] observed peaks at −0.07 and −0.28 eV in FE from Ba atoms singly adsorbed on W(111) as well as a broad peak at about −0.7 eV. It seems likely that their peak at −0.28 eV corresponds to the calculated peak K_3' at −0.32 eV [Fig. 13(b)], while their peak at −0.07 eV may correspond to the calculated peak G_3' at +0.05 eV.

Unoccupied electron states of W(111)/Ba (1×1). Peak H_3' in the K-SDOS of W(111)/Ba (1×1) [Fig. 13(b)] is due to a band of Ba-induced surface resonances [Fig. 13(a)]. The experimentally observed final state peak H_3 (Fig. 12) is attributed to emission from these states. Peak J_3' in the K-LDOS of clean W(111) extends from the central layer of the supercell to the layer beneath the substrate. The experimentally observed final state peak J_3 of clean W(111) and of W(111)/Ba (1×1) (Fig. 12) are attributed to bulk photoexcitation to these states.

In summary, our calculations account for the energies of all of the peaks observed in PFE from W(111)/Ba (1×1) (Table III).

Ba-induced surface reconstruction on W(111). In order to compare the surface electronic structure of W(111)/Ba (1×1) with that of a commensurate overlayer at a lower Ba density, we have also carried out a calculation for W(111)/Ba $(3^{1/2}\times 3^{1/2})R30°$.[22] In both of these structures, the dz^2-like surface resonances close to $\bar{\Gamma}$ that are responsible for the strong asymmetrical peak B_3 at about −0.7 eV in the TED of clean W(111) mix with the *s*-like states of the Ba overlayer to yield a band of surface resonances. For W(111)/Ba $(3^{1/2}\times 3^{1/2})R30°$, the band appears at $\bar{\Gamma}'$ at about −0.9 eV, while for W(111)/Ba (1×1), it appears at $\bar{\Gamma}$ at −1.9 eV and corresponds to the high SDOS at the bottom of the lowest valence band of the isolated Ba (1×1) layer. From the magnitudes of these energy shifts, we conclude that the K-SDOS of the lower-density structure W(111)/Ba $(3^{1/2}\times 3^{1/2})R30°$ is dominated by interlayer W-Ba interactions, while the K-SDOS of the higher-density structure W(111)/Ba (1×1) is dominated by intralayer Ba-Ba interactions.

LEED measurements by Lozovyĭ *et al.*[6] have shown that $(3^{1/2}\times 3^{1/2})R30°$-like islands form on W(111) at low Ba coverage, and fill in to yield an ordered overlayer at 1/3 ML coverage. Above 1/3 ML coverage, the intensity of the $(3^{1/2}\times 3^{1/2})R30°$ LEED pattern decreased, but no new diffraction pattern was observed up to 1.2 ML. The LEED observations, taken together with the present experimental finding that the energy of the surface resonance peak in W(111)/Ba at 1 ML coverage is close to that calculated for

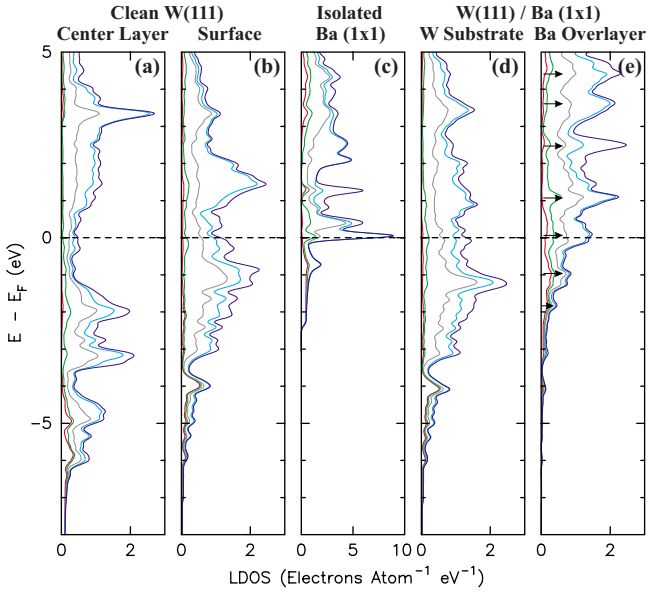

FIG. 14. (Color online) LDOS of clean W(111) in the (a) central (bulk) layer and (b) surface layer. (c) LDOS in an isolated Ba (1×1) layer. LDOS of W(111)/Ba (1×1) in (d) W substrate and (e) Ba overlayer. In these cumulative plots, the areas between successive curves show the contributions of *s*-like (red), *p*-like (green), $dxy+d(x^2-y^2)$-like (gray), $dxz+dyz$-like (light blue), and dz^2-like (dark blue) states, respectively.

W(111)/Ba (1×1), suggest that above 1/3 ML Ba coverage the interstitial sites in the $(3^{1/2}\times3^{1/2})R30°$ structure fill in randomly to yield a (1×1) overlayer at 1 ML coverage.

Work function and LEED data led Lozovyĭ *et al.*[6] to propose that Ba-induced reconstruction of the W(111) substrate may explain why they did not observe a (1×1) LEED pattern at 1 ML coverage. It will be seen from Table III that the energies of the peaks in the TEDs in FE and PFE from W(111)/Ba (1×1), calculated assuming a (1×1) Ba overlayer on a nonreconstructed W(111) substrate, are in good overall agreement with those obtained from experiment. This indicates that the energies of features of the surface electronic structure are not greatly modified by the proposed reconstruction.

B. Layer density of states of clean W(111) and of W(111)/Ba (1×1)

1. Clean W(111)

The strong peaks in the DOS of bulk W at about −3.3 and +3.2 eV [Fig. 14(a)] are greatly attenuated in the surface layer [Fig. 14(b)], while strong surface-induced peaks appear at about −4.0, −1.3, −0.9, and +1.4 eV.

2. Isolated Ba (1×1) layer

The dispersion and the LDOS of an isolated Ba layer were calculated using a supercell in which Ba atoms occupy the same sites as in the W(111)/Ba (1×1) supercell and the W sites are empty. A prominent $d(x^2-y^2)+dxy$ peak appears in the LDOS [Fig. 14(c)] at −0.75 eV, and a very flat *d*, *p* band crosses E_F at close to $\bar{\Gamma}'$, resulting in a prominent $dxz+dyz$-like peak in the LDOS at E_F. Therefore, an isolated Ba (1×1) layer of 4.5 Å lattice constant (0.058 atom Å^{-2}) that is commensurate with W(111) is strongly metallic. This is consistent with electronic structure calculations[46] that show that an isolated hexagonal Ba layer undergoes a metal-to-nonmetal transition at a lattice constant of 5.7 Å (0.036 atom Å^{-2}).

3. W(111)/Ba (1×1)

When the interaction between the substrate and the overlayer is turned on, the surface resonance peaks of clean W(111) at about −4.0, −3.1, and −1.3 eV extend into the overlayer [Fig. 14(e)], the peaks at −0.9 and +1.4 eV are suppressed, and several Ba-induced surface resonance peaks appear, as indicated by arrows in Fig. 14(e). The density of Ba atoms in the isolated overlayer is high (0.058 atom Å^{-2}), resulting in strong metallicity. Interaction with the substrate only slightly enhances the SDOS at E_F, and hence, the metallicity of the overlayer.

C. Work function of W(111)/Ba (1×1)

Experiments[6,47] show that the work function of W(111) decreases to a minimum at 0.6 ML Ba coverage and rises slowly with further Ba deposition. Our experimental FE data[22] show that depositing an unannealed 1 ML Ba overlayer on W(111) at room temperature decreases the work function by 1.8(2) eV. This is consistent with the decrease of about 2.0 eV (Ref. 6) reported in the literature for similar experimental conditions. Our calculations show that the work function of W(111)/Ba (1×1) is less than that of clean W(111) by 2.0(1) eV.

VII. CONCLUSIONS

The TEDs in FE and PFE and the work functions of W(100), W(110), and W(111) with adsorbed Ba overlayers have been measured in the range of coverage from 0 to 1 ML on W(100), from 0 to 0.6 ML on W(110), and from 0 to 1.0 ML on W(111). Our calculations account for the energies of all of the well-resolved peaks observed experimentally in the TEDs in FE from clean W(100), in PFE and in ARIPS from W(100)/Ba $c(2\times2)$ (Table I), in PFE and photoemission from W(110)/Ba (2×2) (Table II), and in PFE from W(111)/Ba (1×1) (Table III).

The Swanson hump B_1 in the TEDs of FE and PFE from clean W(100) is suppressed by as little as 0.1 ML coverage of Ba. The surface states that are responsible for the Swanson hump hybridize with the valence states of the Ba $c(2\times2)$ overlayer to form extended surface states that give rise to the prominent initial state peak F_1 and the initial state peak G_1 observed in PFE.

When a $c(2\times2)$ overlayer is adsorbed on a square (1×1) substrate, the symmetry point $\bar{M}$ in the SBZ of the substrate is folded back to $\bar{\Gamma}'$ in the SBZ of the overlayer, enabling states at $\bar{M}$ in the SBZ of the substrate to contribute

to FE and PFE. This effect accounts for the weak final state peak J_1 that is observed experimentally in the TED in PFE from W(100)/Ba $c(2\times2)$.

Our electronic structure calculations for an isolated Ba $c(2\times2)$ layer show that there is only a slight overlap between the lowest *s*-, *p*-, and *d*-like bands, resulting in weak metallicity. In W(100)/Ba $c(2\times2)$, the interaction with the substrate greatly increases the metallicity of the overlayer.

While the total charge within a Ba muffin-tin sphere remains unchanged when Ba is adsorbed as a $c(2\times2)$ overlayer on W(100), the charge is redistributed among the angular momentum states, modifying the spatial distribution of charge in the vicinity of the surface. This results in a strong outwardly directed dipole layer between the substrate and the overlayer, and a weak inwardly directed dipole layer outside the surface. The work function decrease calculated from the surface dipole layers induced by a Ba $c(2\times2)$ overlayer on W(100) is in good agreement with the experimentally observed work function decrease at 1 ML coverage.

When a (2×2) overlayer is adsorbed on a rectangular (1×1) substrate, the symmetry point $\bar{S}$ in the SBZ of the substrate is folded back to $\bar{\Gamma}'$ in the SBZ of the overlayer, so that states at $\bar{S}$ in the SBZ of the substrate can make a significant contribution to FE and PFE. This effect accounts for the experimentally observed peak H_2 in the TED in PFE from W(110)/Ba (2×2).

The peaks observed in the experimental TED are significantly wider than the calculated peaks. Our results for clean W(100) suggest that discrepancies in the relative strengths of the emission peaks are dominated by lifetime broadening due to scattering by defects at the emitting surface. It seems likely that any additional discrepancies in the relative strengths of the peaks in surface PFE are due to our simplified treatment of the surface photoexcitation matrix element of Schwartz and Cole.[38]

Our calculation for clean W(111) yields two bands of surface resonances B_3' and C_3' of predominantly dz^2-like symmetry that straddle the prominent asymmetrical FE peak B_3 at −0.65 eV. Overlapping of the peaks B_3' and C_3' due to strong lifetime broadening offers a natural explanation for the experimentally observed asymmetry of peak B_3.

Peak B_3 is suppressed by as little as 0.03 ML Ba coverage. Hybridization with the lowest *s*-like valence states of the Ba (1×1) overlayer shifts the surface resonances B_3' and C_3' of clean W(111) to lower energy, yielding strong peaks F_3' in the K-SDOS and in the TED in PFE.

For W(110)/Ba (2×2) and W(111)/Ba $(3^{1/2}\times3^{1/2})R30°$, with atomically less dense Ba overlayers, the K-SDOS in the overlayer is closely related to the K-LDOS in the substrate, and hence, the TED in PFE is dominated by substrate-overlayer interactions, while for W(111)/Ba (1×1), with an atomically denser overlayer, the K-SDOS of W(111)/Ba (1×1) is closely related to the LDOS in the isolated overlayer, and hence, the TED in PFE is dominated by interactions within the overlayer.

Electronic structure calculations for an isolated Ba (2×2) layer commensurate with W(110) show a small density of states (DOS) at E_F, implying weak metallicity. When a Ba (2×2) overlayer is adsorbed on W(110), its metallicity is greatly enhanced by the interaction with the substrate. An isolated Ba (1×1) layer commensurate with W(111) shows a large DOS at E_F, and hence, strong metallicity. When a Ba (1×1) layer is adsorbed on W(111), its metallicity is only slightly enhanced by interaction with the substrate.

The work function reductions calculated from the charge shifts induced by a Ba (2×2) overlayer on W(110) and by a Ba (1×1) overlayer on W(111) are in good agreement with those measured experimentally at room temperature by FE from unannealed overlayers.

By comparing the electron emission TEDs and work function data with the results of our calculations, we conclude that DFT with exchange and correlation treated in the GGA is adequate to describe the surface electronic structure of Ba adsorbed on low-index facets of W.

The method of calculation described in the present work can be readily applied to the low-index surfaces of a wide range of materials to determine the TEDs in FE and PFE, the energies and symmetries of electronic states at metallic surfaces, the modification of the electronic structure in going from the surface to the bulk, and the charge shifts that accompany the adsorption of a commensurate overlayer.

ACKNOWLEDGMENTS

We are indebted to T. Radoń for helpful discussions. One of us (Z.A.I.) wishes to acknowledge partial financial support from the University of Toronto, the Natural Sciences and Engineering Research Council of Canada (NSERC), and the government of Ontario (OGS). This work was supported in part by an NSERC Discovery Grant.

*Corresponding author; zahraa.ibrahim@uoit.ca

[1] A. Lamouri and I. L. Krainsky, Surf. Sci. **278**, 286 (1992).
[2] D. A. Gorodetsky and Y. P. Melnik, Surf. Sci. **62**, 647 (1977).
[3] B. J. Hopkins and B. J. Smith, J. Chem. Phys. **49**, 2136 (1968).
[4] A. G. Fedorus, A. G. Naumovets, and Y. S. Vedula, Phys. Status Solidi A **13**, 445 (1972).
[5] V. K. Medvedev, Sov. Phys. Solid State **10**, 2752 (1969).
[6] Y. B. Lozovyĭ, V. K. Medvedev, T. P. Smereka, G. V. Babkin, B. M. Palyukh, and O. S. Vasil'chishin, Sov. Phys. Solid State **28**, 2080 (1986).
[7] H. Utsugi and R. Gomer, J. Chem. Phys. **37**, 1706 (1962).
[8] G. E. Moore and H. W. Allison, J. Chem. Phys. **23**, 1609 (1955).
[9] A. G. Naumovets, V. V. Poplavsky, and Y. S. Vedula, Surf. Sci. **200**, 321 (1988).
[10] E. W. Plummer and R. D. Young, Phys. Rev. B **1**, 2088 (1970).
[11] J. W. Gadzuk, Phys. Rev. B **1**, 2110 (1970).
[12] T. Radoń and S. Jaskólka, Acta Phys. Pol. A **87**, 657 (1995).
[13] A. Lamouri, W. Müller, and I. L. Krainsky, Phys. Rev. B **50**,

4764 (1994).
[14] T.-W. Pi, I.-H. Hong, and C.-P. Cheng, Phys. Rev. B **58**, 4149 (1998).
[15] T.-W. Pi, I.-H. Hong, R.-T. Wu, and C.-P. Cheng, Surf. Rev. Lett. **4**, 1197 (1997).
[16] L. A. Hemstreet and S. R. Chubb, Phys. Rev. B **47**, 10748 (1993).
[17] Miniature K-cell Effusion Source, Model WKC-2G, W. A. Technology, Cambridge, UK.
[18] D. Venus, Ph.D. thesis, University of Toronto, 1985.
[19] P. J. Donders, K. W. Hadley, and M. J. G. Lee, Rev. Sci. Instrum. **56**, 2074 (1985).
[20] G. A. Gaudin and M. J. G. Lee, Surf. Sci. **280**, 91 (1993).
[21] G. Gaudin, Ph.D. thesis, University of Toronto, 1993.
[22] Z. A. Ibrahim, Ph.D. thesis, University of Toronto, 2006.
[23] Innova 90 krypton ion laser, Coherent Inc.
[24] R. H. Fowler and L. W. Nordheim, Proc. R. Soc. London, Ser. A **119**, 173 (1928).
[25] L. W. Nordheim, Proc. R. Soc. London, Ser. A **121**, 626 (1928).
[26] A. Shih, G. A. Haas, and C. R. K. Marrian, Appl. Surf. Sci. **16**, 93 (1983).
[27] Karlheinz Schwarz, WIEN2K, An augmented plane wave + local orbitals program for calculating crystal properties (Technical University of Wien, Austria, 2001).
[28] J. P. Perdew, J. A. Chevary, S. H. Vosko, K. A. Jackson, M. R. Pederson, D. J. Singh, and C. Fiolhais, Phys. Rev. B **46**, 6671 (1992).
[29] A. Modinos and N. Nicolaou, Phys. Rev. B **13**, 1536 (1976).
[30] M. J. G. Lee and Z. A. Ibrahim, Phys. Rev. B **70**, 125430 (2004).
[31] P. E. Blöchl, O. Jepsen, and O. K. Andersen, Phys. Rev. B **49**, 16223 (1994).
[32] J. P. Vigneron and Ph. Lambin, J. Phys. A **13**, 1135 (1980).
[33] Ph. Lambin and J. P. Vigneron, J. Phys. A **14**, 1815 (1981).
[34] H. Q. Nguyen, P. H. Cutler, T. E. Feuchtwang, N. Miskovsky, and A. A. Lucas, Surf. Sci. **160**, 331 (1985).
[35] R. D. Young, Phys. Rev. **113**, 110 (1959).
[36] A. Modinos, *Field, Thermionic, and Secondary Electron Emission Spectroscopy* (Plenum, New York, 1984), Chap. 5.
[37] J. W. Gadzuk and E. W. Plummer, Rev. Mod. Phys. **45**, 487 (1973).
[38] C. Schwartz and M. W. Cole, Surf. Sci. **115**, 290 (1982).
[39] J. C. Slater, *Quantum Theory of Molecules and Solids* (McGraw-Hill, New York, 1965), Vol. 2.
[40] L. W. Swanson and L. C. Crouser, Phys. Rev. Lett. **16**, 389 (1966).
[41] E. W. Plummer and A. E. Bell, J. Vac. Sci. Technol. **9**, 583 (1972).
[42] Z. A. Ibrahim and M. J. G. Lee, Prog. Surf. Sci. **67**, 309 (2001).
[43] G. A. Katrich, V. V. Klimov, and I. N. Yakovkin, Ukr. J. Phys. **37**, 429 (1992).
[44] P. A. Dowben, D. LaGraffe, D. Li, G. Vidali, L. Zhang, L. Dottl, and M. Onellion, Phys. Rev. B **43**, 10677 (1991).
[45] E. W. Plummer and P. A. Dowben, Prog. Surf. Sci. **42**, 201 (1993).
[46] I. N. Yakovkin, Surf. Sci. **442**, 431 (1999).
[47] L. D. Schmidt, J. Chem. Phys. **46**, 3830 (1967).
[48] R. L. Billington and T. N. Rhodin, Phys. Rev. Lett. **41**, 1602 (1978).